Fall 8-20-2019

Tailored Frequency Comb Structures and Their Sensing Applications

James Hendrie
University of New Mexico - Main Campus

James Philip Hendrie

Candidate

Optical Science and Engineering

Department of Physics and Astronomy, The University of New Mexico

This dissertation is approved, and it is acceptable in quality and form for publication:

Approved by the Dissertation Committee:

Dr. Jean-Claude M. Diels, Chair

Dr. Francisco Elohim Becerra

Dr. Ladan Arrissian

Dr. R. Jason Jones

Dr. Wolfgang Rudolph

Tailored Frequency Comb Structures and Their Sensing Applications

by

James Philip Hendrie

B.S., Indiana University, 2012
M.S., University of New Mexico, 2015

DISSERTATION

Submitted in Partial Fulfillment of the
Requirements for the Degree of

Doctor of Philosophy
Optical Science and Engineering

The University of New Mexico

Albuquerque, New Mexico

December 2019

https://orcid.org/XXXX-XXXX-XXXX

Dedication

To my family and friends who have stood by me and supported me in ways that I can never fully repay. This is for you.

We can easily forgive a child who is afraid of the dark; the real tragedy of life is when men are afraid of the light.

– Plato

Acknowledgments

This dissertation and the work presented within it would not have been accomplished without the overwhelming support of my family, friends, professors, staff, and colleagues, as well as funding from NASA and NSF. There is not nearly enough space to adequately thank all of them individually, so instead I would like to highlight those who have been of particular importance to this specific project.

Firstly, my advisor and mentor, Dr. Jean-Claude Diels who has supported me financially and academically throughout my time here. Dr. Diels has taught me the importance of methodical and patient experimentalism. He has allowed me to chase down projects that I thought were interesting, even when they did not lead to publishable results, which has helped me learn about optics in a truly open environment. He has also been a friend and advisor, helping me through some trying personal times and enjoying many off topic conversations and mountain adventures. I could not have asked for a more knowledgeable, intelligent, and supportive dissertation advisor.

I would also like to thank Dr. Matthias Lenzer and Dr. Marvin Morris who have helped me countless times with working out tricky alignments and computer issues. Lenzer helped me to design and construct a variety of specialized mounts and both were eager council when it came to discussing my future in science.

Thank you to Dr. Elohim Becerra has been a lab neighbor and advisor on many aspects of my project and graciously agreed to be on my committee, and to Dr. Ladan Arissian who helped me through many discussions on frequency combs and was always there to help with publications and presentations.

I will always cherish my friends that I have met here in Albuquerque, though there are definitely too many of you to name. That being said, my roommates Megan Lewis, Jacek Osinski, and Eric Bahr have been amazingly understanding and helpful, and Dr. Adrian Chapman, who lived with me for 5 years, every night we were up till 2 or 3 in the morning proofing papers and talks and discussing results has finally lead to our both graduating, and I would not trade a moment of it.

Finally, thank you to my parents, Drs. Jennie and Paul Hendrie, my brother, Dr. Kyle Hendrie, his wife, Zariah Hendrie, my grandparents, Drs. Hugh and Marguerite Hendrie, Captain Philip Gubbins, and Dr. Christine Gubbins, and my girlfriend Carolina Bucheli, for all the countless hours of counseling, proof reading, and unwavering support all of you have given to me without a second thought.

Tailored Frequency Comb Structures and Their Sensing Applications

by

James Philip Hendrie

B.S., Indiana University, 2012
M.S., University of New Mexico, 2015

Ph.D., Optical Science and Engineering, University of New Mexico, 2019

Abstract

The focus of this doctoral dissertation is the development and investigation of nested cavity mode-locked lasers and their resultant tailored frequency combs. A nested cavity is made up of two cavities, known as parents. One parent is a larger, active, 100MHz Ti:Saph oscillator and the other is a smaller, passive, 7GHz Fabry-Perot Etalon (FPE). Unlike standard frequency combs that are continuous, a tailored comb's teeth are distributed in equally spaced groups where the center of each group corresponds to the resonance of the FPE and the side bands are determined by the resonances of the Ti:Saph. This unique coupling of the MHz and GHz resonances opens the door to a wide variety of applications.

One such application is the enhancement of Intracavity Phase Interferometry (IPI). IPI is a technique in which two pulses propagate within a shared active oscillator. These pulses experience a difference in phase, $\Delta\phi$, which results in a frequency comb shift of $\Delta\omega = \frac{\Delta\phi}{\tau_{RT}}$, where τ_{RT} is the round-trip time of the oscillator, relative to one another. $\Delta\omega$ is measured as a beat-note signal when the two pulses are interfered and can be resolved at less than a kHz value with Hz resolution. Nested cavities

were introduced into this technique to further enhance the beat-note signal. The enhancement comes from the fact that the frequency group locations in a tailored comb are set by the passive parent's optical properties, which are frequency dependent. Therefore, $\Delta\omega$ increases as the FPE's linear dispersion further separates the two combs. While this dissertation will focus on IPI as it relates to gyroscopes, it has also been demonstrated in magnetic field and n_2 measurements.

The successful demonstration of IPI enhancement, along with the characterization and stability of tailored combs, are presented and discussed.

Contents

List of Figures

List of Symbols

Presented in the order of appearance.

$E_k(i)$	Electric field of pulse i at round trip$k$ through an etalon
i	An index of numbers
k	An index of numbers, or the wave number
R	Intensity reflection coefficient
γ_i	Loss factor per round trip, i
γ_0	Initial loss factor
a	Loss factor due to the tilting of an etalon
i_c	Index of the central most pulse
$\frac{dG}{dt}$	Cavity staturable gain rate
G	Amount of gain per pulse
W	Pulse energy
W_S	Saturation energy
I_S	Saturation intensity
T_1	Population inversion recover time
G_e	Equilibrium gain for the case of no stimulated emission
E_s	Saturated electric field
v_p	Phase velocity
c	Speed of light
n_p	Phase index
Ω	Variable optical angular frequency

v_g	Group/Pulse velocity
n_g	Group/Pulse index
ω	Angular optical frequency
v_B	Bunch velocity
n_B	Bunch index
ν_C	Laser cavity repetition rate
L	Laser cavity length
ν_{FPE}	Fabry-Perot etalon repetition rate
d	Fabry-Perot etalon length
θ	Fabry-Perot etalon internal angle
ω_0	Central angular optical frequency
N_{FPE}	The number modes supported by the etalon
N_C	The number of modes supported by the laser cavity
f_N	The frequency value of a comb tooth specified by an index
f_{CEO}	Carrier envelope offset frequency
N	A frequency index
$f_{Rep.Rate}$	Repetition rate frequency
f_{Offset}	Comb offset frequency
M	A frequency index or summing index
f_{FPE}	Repetition frequency of a nested etalon
f_P	Repetition frequency of a parent cavity
λ	Optical wavelength
ν_C	Repetition rate larger cavity
ν_{FPE}	Repetition rate of the nested etalon
$\mathcal{R}$	Ratio of the larger cavity repetition rate to the nested etalon repetition rate
N_C	Number of optical modes supported by the larger cavity
N_{FPE}	Number of optical modes supported by the nested etalon
I	Nearest integer value of the repetition frequency ratio of a nested cavity system
δ	Fractional offset from an integer or a phase term

$\bar{\delta}$ Average value of the fractional numerical value from a whole integer, I of the repetition frequency ratio of a nested cavity system

Δ The variance of the fractional numerical value from a whole integer, I of the repetition frequency ratio of a nested cavity system

$\mathfrak{R}$ The super ratio; aka, the ratio of an initial $\mathcal{R}$ to an $\mathcal{R}$ of a modified cavity at the same etalon location

$\Delta n_{p,FPE}$ The change in the refractive index of the nested etalon

α_T Refractive index thermal coefficient, dn/dT; where n is the phase index and T is temperature

$\Delta\omega$ Measured beat note

$\Delta\phi$ Overall phase difference between two combs

τ_{RT} Round trip time within a cavity

ΔP Apparent change in cavity perimeter

P Cavity perimeter

λ_C Central wavelength

$\mathbf{\Omega}$ Rotational velocity

$\mathbf{A}$ Directional area

$\left.\frac{d\psi}{d\Omega}\right|_{\omega_0}$ Linear dispersion

$\Delta\omega_0$ Initial beat note without enhancement

r The square root of the reflectivity of the front face of an etalon

r' The square root of the reflectivity of the back face of an etalon

α Simplifying variable

β Simplifying variable

γ Simplifying variable

σ_{Allan} Allan deviation

ν Frequency

$< \nu >$ Average frequency

τ Time span of averaging

List of Acronyms

Presented in the order of appearance.

CW	Continuous Wave
HeNe	Helium Neon
Fig.	Figure
FPE	Fabry-Perot Etalon
IPI	Intra-cavity Phase Interferometry
Ti:Sapph	Titanium Sapphire
MQW	Multiple Quantum Well
Eq.	Equation
RT	Round Trip
APD	Avalanche Photo Diode
rf	radio frequency
GHz	Giga-Hertz
MHz	Mega-Hertz
Rep.Rate	Repetition Rate
Hz	Hertz
CCD	Charge-Coupled Device
ML	Mode-Lock
^{87}Rb	Rubidium 87
NIST	National Institute of Standards and Technology
PMT	Photo Multiplier Tube

Det.	Detector
hrs.	Hours
CEO	Carrier Envelope Offset
DFG	Difference Frequency Generation
^{o}C	Degrees Celsius
CLEO	Conference on Laser and Electro Optics
SPM	Self Phase Modulation
SHG	Second Harmonic Generation
OC	Output Coupler
OPO	Optical Parametric Oscillator
SA	Saturable Absorber
RLG	Ring Laser Gyroscope
cw	Clockwise
ccw	CounterClockwise
kHz	Kila-Hertz
V	Volts
GTI	Gires Tournois Interferometer
AR	Anti-Reflection
PBS	Polarizing Beam Splitter
TGG	Terbium Gallium Garnet
NASA	National Aeronautics and Space Administration

Chapter 1

Introduction

> Light thinks it travels faster than anything but it is wrong. No matter how fast light travels, it finds the darkness has always got there first, and is waiting for it.
>
> – Terry Pratchett, Reaper Man

1.1 Introduction

This beginning chapter serves to introduce the topics of mode-locking and frequency combs as a motivation of the concept of "tailored frequency combs", which will be the main topic of this dissertation. A frequency comb is an equally rigidly spaced collection of narrow frequency teeth generated by a continuous train of pulses. In this case, those pulses are generated by a mode-locked oscillator. A brief history of optical frequency combs will also be provided. It should be noted, crucially, that this invention of a tailored comb, that can be deterministically modulated, in no way decreases the stability and rigidity of the frequency comb as a whole, and therefore, the optical comb maintains its place as a uniquely important tool as a frequency reference and measure. In fact, much like the analogy of calipers to a ruler, the tailored comb takes the accuracy of its predecessor and adds a level of precision

and malleability that its inflexible predecessor lacks. This dissertation will discuss the latest results in the characterization of these combs as well as their utility in various metrology experiments. While this dissertation does not serve as a final review of nested combs, hopefully it serves as an end to their preliminary study and the motivation for in depth studies of their stabilization and usefulness in enhancing comb sensing techniques.

1.2 A Brief History of Frequency Combs and Their Advancements

The history of the laser is relatively short as far as areas of physics go; however, it is still much to long to be contained in the introductory chapter of a dissertation. Rather than include an exhaustive history, this manuscript will simply provide a brief look at how optical combs have come about and where they were traditionally used.

The first Continuous Wave (CW) Helium Neon (HeNe) Laser was demonstrated in 1960. Since this time, lasers have been used and studied for their ability to have stable frequencies and to measure time via the speed of light. In 1976, time-periodic pulses were used to generate a frequency comb, essentially demonstrating a cavity with multiple co-oscillating frequency modes whose spacing is determined by the cavity [1]. In order to stabilize these combs, which was necessary to achieve a useful frequency ruler, it was necessary to broaden the spectra produced by these lasers. Femto-second pulses were achieved in 1980 [2][3][4], which allowed for a much broader comb that could then be broadened even more to directly connect the optical frequency to a radio frequency standard in 1999 [5]. In order to directly measure, and therefore stabilize these combs, two comb teeth of at least one harmonic spacing, or one octave apart, must be compared.

With this ultimate stabilization, many applications became available for these combs in the form of dual comb spectroscopy as well as metrology and even as frequency reference applications, such as astro-combs, used to look at the shifted spectra of astronomic bodies [6][7]. Intra-cavity Phase Interferometry [8], which will be discussed in detail in chapter 3, is another technique that was first invented in the 1990's [9][10]. Enhancement of this technique is the ultimate goal of this dissertation. Therefore, more details into how it works and how a modular comb can be used to affect its phase response will be discussed further in chapter 3.

Today, atomic clocks using frequency comb references have been stabilized to 10^{-11} instability [11], and more recently, some combs have even been stabilized to 10^{-18} [12]. This incredible precision would seem to indicate a near complete understanding of optical combs; however, with new and unique tailored combs and their many interesting characteristics, it is clear we have only scratched the surface of possibilities for frequency combs.

1.3 Mode-locking and Frequency Combs

The concept of mode-locking a laser and the generation of optical frequency combs are uniquely tied. In brief, mode-locking is achieved when the supported frequencies of a given cavity become locked together in phase, such that the frequencies add constructively at one cavity location to produce a pulse of light. These pulses then exit the cavity with a constant spacing between each consecutive pulse dictated by the cavity repetition rate. This pulse train's Fourier transform forms a comb in the frequency domain whose teeth are essentially sidebands created by this constant repetition rate. This is different from the typical CW laser operation in that only one frequency mode is produced in that case and it is solely determined by the effective index and length of the cavity. In this case, the available cavity modes for CW operation are not equally spaced, and only one survives.

These combs act as "fingerprints" [8] of their generating cavities, which makes these are cavities capable of very precise sensing. The slightest change of air pressure, temperature, or cavity alignment results in a measurable shift in the value of the supported frequencies and their spacing. It then becomes obvious that, the better one can measure these changes in a comb structure, the better the sensitivity that these natural laser sensors can provide.

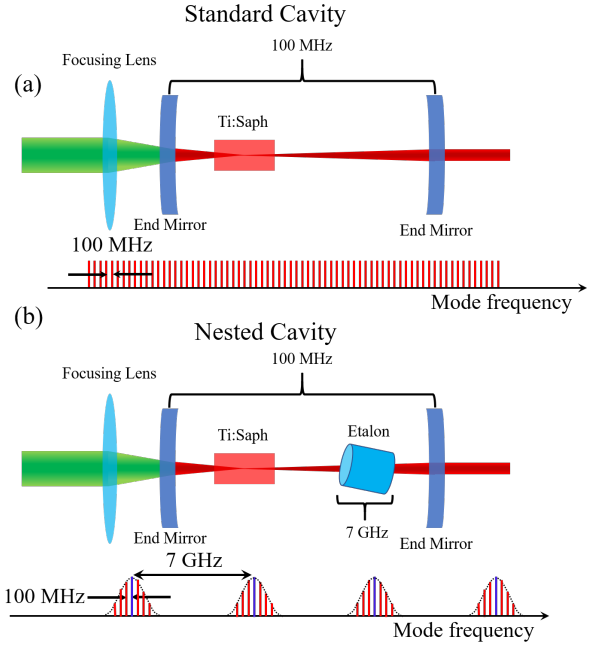

Figure 1.1: An introductory schematic which illustrates the difference in design and in frequency domain output of a standard linear Ti:Sapph cavity, (a), and a nested cavity, (b).

This dissertation will focus on two unique advancements in laser comb technology. The first is a new type of modular comb, first discovered by my predecessor, Dr. Koji Masuda, known as a *tailored comb*. This comb is the product of *nesting* a passive cavity within an active one as shown in Fig. 1.1. Part (a) of this illustration, a typical mode-locked Ti:Sapph cavity is depicted with its typical comb below it. The repetition rate of this comb is set by the repetition rate of the cavity, as shown in the figure. In part (b), the same cavity is shown, only this time a passive Fabry-Perot

etalon (FPE) has been placed inside (shown at an exaggerated angle). Below this cavity is shown the generated comb, whose frequency groups are separated by the repetition rate of the passive etalon, while the side bands correspond to the laser repetition rate, just as in part (a).

The tailored comb introduced above is produced in these nested cavities, and manifests itself in pulse bunches rather than a single pulse, circulating in the cavity at the round trip time. Fig. 1.2 uses a real oscilloscope trace (top) and a real radio frequency spectrum analyzer trace (bottom) to show how the time and frequency domain of these combs are related. In chapter 2, I will focus on the definition and

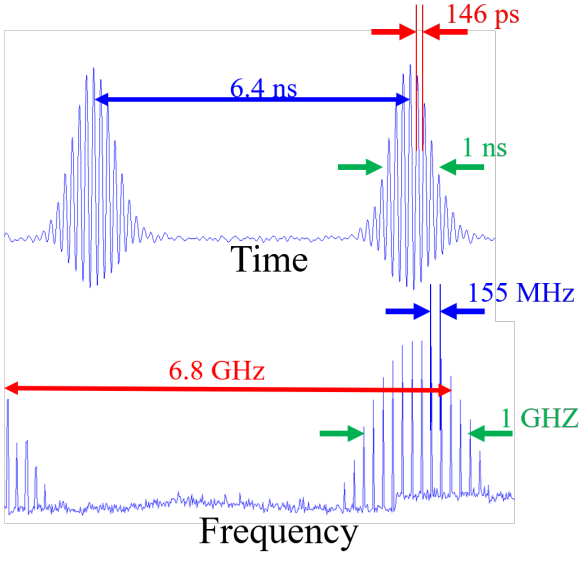

Figure 1.2: This figure is made of up an actual oscilloscope trace (top) and an actual radio frequency spectrum analyzer trace (bottom) to represent and explain the connection between the time and frequency domains. In the time domain, the blue text shows the laser cavity round trip time, the green text shows the Full Width Half Max (FWHM) of the generated bunches, and the red text shows the separation of the pulses within the bunch, which corresponds to the round trip time of the Fabry-Perot Etalon (FPE). These colors are preserved in the frequency picture to show how the time domain values correspond to frequencies. These experimental results can be easily confirmed via Fourier transforms.

generation of these combs and bunches as well as their characterization and possible applications.

The second innovation is an enhancement of a frequency comb metrology technique known as Intra-cavity Phase Interferometry (IPI). In chapter 3 I explain this method and its history, and then detail how its already high level of sensitivity can be enhanced, or reduced, by the introduction of resonant linear dispersion, achieved via a passive etalon. Experimental results of the proof of concept experiment will be provided, along with the first observed enhancement and a description of how to achieve even greater enhancement via future methods. Chapter 4 will conclude this dissertation with some closing remarks about these technologies as well as their future applications and possible further advancements.

Chapter 2

Tailored Combs

2.1 Introduction

The primary focus of this chapter is on the nesting of passive cavities inside active parents, which is done to create nested, or tailored combs. This chapter will define and characterize the phenomena of nested combs and discuss their various processes. First, the design and construction of what is known as a nested cavity will be presented. Then a description of the resultant pulse bunch train in the time domain, and a complete description of the frequency domain and definition of a tailored combs will be given. Finally, discussions of the tuning, stability, and applications will be provided.

2.2 Design and Construction of Nested Cavities

A nested cavity, for the purposes of this work, is created by the insertion of a passive *nested* Fabry-Perot etalon[1](FPE) into an active mode-locked laser *parent* cavity. Every parent cavity throughout this dissertation is a Titanium Sapphire (Ti:Sapph) laser; though, in principle, any mode-locked cavity could be modified in this nested

[1]An etalon is a solid, optically transparent, object with parallel faces.

cavity manner.

The construction of one of these nested cavity lasers is done simply by inserting the *nested* cavity into the *parent*. The process that yields the best results is to first mode-lock the parent cavity at the desired wavelength and lower the pumping threshold as much as possible. This is desirable since the act of nesting an etalon will result in an increase in the total loss of the laser. Once a low threshold is achieved, insert the *nested* cavity and align it such that the multiple reflections are visible and form a straight line[2] from out of the output coupler of the laser. The laser will not be lasing at this point, so what you are aligning is simply the spontaneous emission of the gain. It is also easier to keep these reflections close to the central emission spot as these nested cavities are easier to get lasing at angles closer to zero to begin with. Once this is completed, the power should be increased until lasing is achieved. There may be some small alignment necessary in the cavity to regain mode-locking, but this should be minimal. Getting nested cavity mode-locking at higher angles is usually just a matter of increasing the pump power and minor adjustments to the cavity focusing mirrors. An example cavity is depicted in Fig.2.1.

While certain elements that were utilized in later experiments are omitted from this cavity, this illustration shows the fundamental components necessary for nested cavity mode-locking. In this design, the mode-locking mechanism is a Multiple Quantum Well (MQW); however, unlike the standard version of this cavity, the prisms and MQW are located in the same arm, leaving the nested cavity in an arm by itself. This was done for two reasons. First, it is best if the laser is collimated in the arm with the nested cavity, though not necessary. Second, this allows for easier access to the motors and other equipment that is invariably attached to the nested cavity for the purpose of exploring its effects.

[2]The straight line can be in either the vertical or horizontal direction, depending on the direction of tuning to be used later.

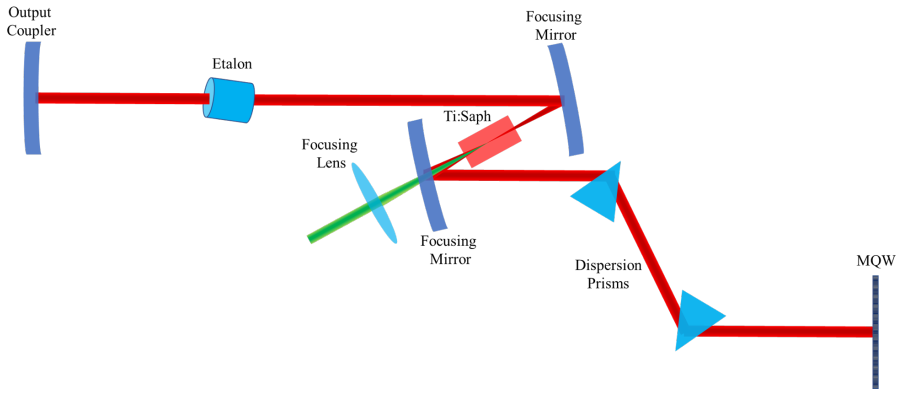

Figure 2.1: A schematic of a linear Ti:Sapph laser cavity is shown with a Fabry-Perot etalon (FPE) nested inside to generate a stable tailored frequency comb. This cavity is mode-locked via a Multiple Quantum Well (MQW) and is dispersion controlled via a prism pair.

Later in this chapter the effect of the optical and physical properties of the nested cavity will be discussed, but for now, it should be noted that the faces of the etalon account for a substantial amount of loss within this type of cavity. The greater the angle of the nested cavity, the greater the loss factor, which should be considered when designing such a cavity.

2.3 Nested Cavities in Various Domains

Nested cavities generate unique and modular features in both the frequency and time domains. This section serves to describe these and provide depictions to help visualize and understand them.

2.3.1 Dynamics of Time Domain Pulse Bunches

In the previous section, a simple description of the necessary alignment of nested cavities was laid out. With this understanding of the set up, this section will serve to explain the time domain picture of the pulses within the cavity, how they interact,

and their various characteristics. Fig.2.2 illustrates the process by which pulses within a pulse bunch interact within a nested FPE.

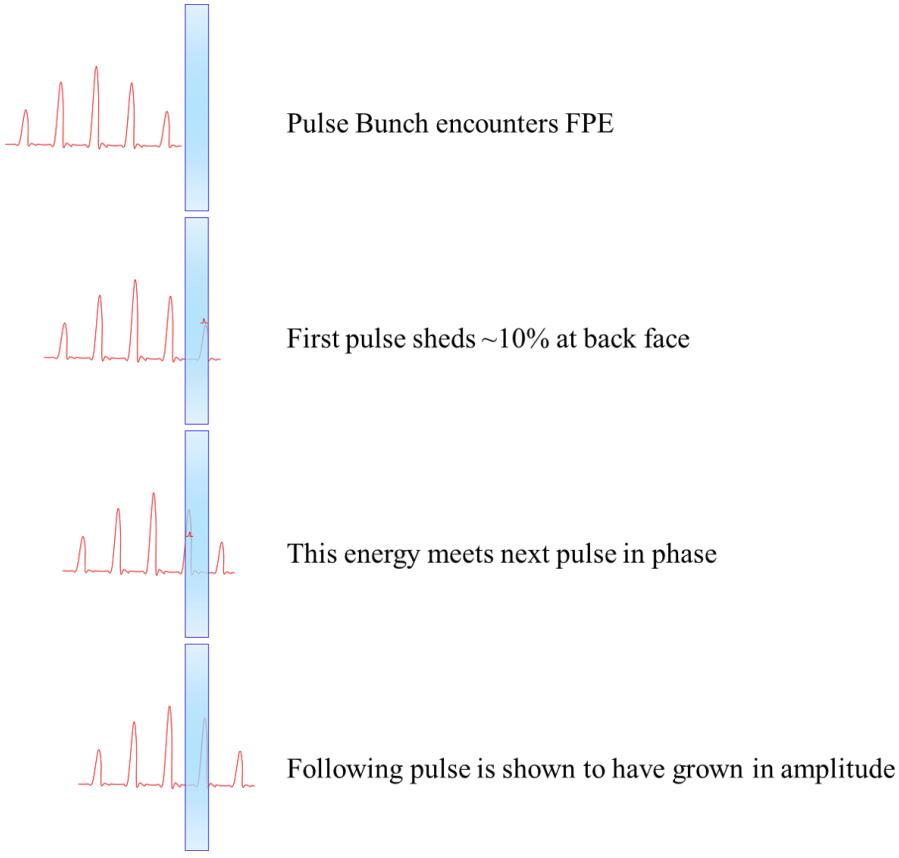

Figure 2.2: Shows the exchange of energy of pulses passing through FPE. FPE is shown as vertical for convenience since the angles that are used are typically at the single to tens of mili-radian level.

As shown in Fig. 2.2, as a pulse bunch comes in contact with the etalon, each pulse sheds a small amount of energy to the next one, proportional to its individual intensity, which is coherently added to the next pulse in the bunch. Note, no two pulses are ever completely inside the FPE at the same time. In this way, there is a constant attenuation of pulses at the front of the bunch and an amplification of pulses at the back of the bunch causing this steady and stable pulse bunch envelop to house a constantly evolving pulse group. This pulse energy shearing can be described by;

$$E_k(i) = (1 - R) \sum_{j=i}^{j=1} [R^{i-j} E_{k-1}(j)], \tag{2.1}$$

where E is the electric field and R is the intensity reflection coefficient.

It is also important to include a loss factor, γ, per round trip, given by;

$$\gamma_i = \gamma_0 + a(i_c - i)^2, \tag{2.2}$$

where a is the loss factor due to the tilting of the FPE and i_c is the index of the central most pulse.

This interaction of pulses within a given bunch is only part of the process of creating a stable bunch. Another key element is the idea of saturable gain. Saturable gain is the idea that, for a short period of time, the amount of gain in an active cavity, such as a laser, is finite and pulses within this cavity receive gain proportional to their amplitude. This concept is very important in this particular cavity, to the point where attempting to model this cavity without including saturable gain leads to unstable solutions.

As noted above, it is crucial to include saturable gain in these calculations. To that end, we first define the saturable gain rate for a ps pulse per round trip;

$$\frac{dG}{dt} = -\frac{GW}{W_s T_1} - \frac{G - G_e}{T_1}, \tag{2.3}$$

where G is the amount of gain per pulse of energy W. The saturation energy is given by $W_s = I_s T_1$, where I_s is the saturation intensity and T_1 is the inversion recovery time, known to be on the order of micro-seconds, much slower than the standard repetition rate of the cavities used in this work. Finally, G_e is the equilibrium gain for the case of no stimulated emission. With this in hand, we then can define the gain depletion for this type of cavity via;

$$G_k(i) - G_k(i-1) = -\frac{G_k(i-1)E_k^2(i-1)}{E_s^2 T_1} - \frac{G_k(i-1) - G_e}{T_1}. \tag{2.4}$$

Here, i is the pulse index and k is the round trip index. Fig.2.3 shows the results of a simulation published in [13] which illustrates how a cavity can be modeled in this

way to reach a steady state pulse bunch.

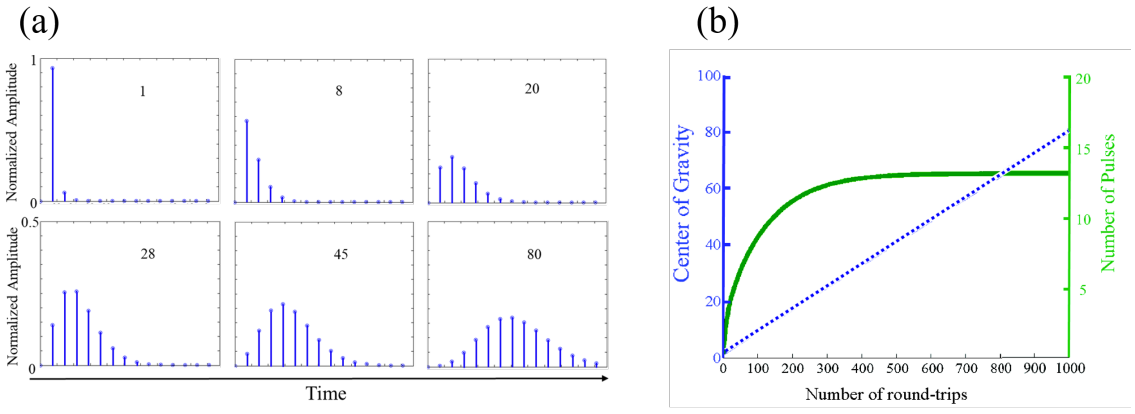

Figure 2.3: Results of a simulation, published in [13], demonstrating the move of a nested cavity to a steady state mode of operation. In part (a), the simulation starts at round trip 1, the number label within the left most upper panel, with a single pulse. As the simulation progresses, more pulses are generated until a steady condition is reached around round trip 80. It is seen here that the shape of this time domain pulse bunch has a Gaussian envelope. In part (b), we see how the center of gravity of a pulse bunch shifts per round trip and how the number of pulses per bunch quickly stabilizes.

While this simplistic simulation had some shortcomings; in actuality, the assumption that a laser would create a single pulse first and then use it to generate more pulses is a bit of a stretch. It is enough to demonstrate two important characteristics of pulse bunches within these cavities. First, the condition of pulse bunch mode locking is a viable steady state condition for the laser, even though individual pulses within the bunch experience constant energy shifts per round trip (RT). Second, these bunches invariably obtain a Gaussian envelope when they reach their steady state. While the latter point is more cosmetic in nature, though nice when attempting to write simulations for the frequency domain, the former is a bit more subtle. Typically, when a cavity is said to be in steady state, the electric field of the pulse is recreated exactly every RT. In the case of pulse bunches, it is true that a Gaussian bunch of pulses is produced each RT; however, a specific pulse contained within that bunch changes both in energy and position under the bunch envelope. This leads to a "dynamic" steady state, with the bunch appearing to propagate at a lower velocity. This important point leads to the necessity to define a new set of parameters that

describe these unique bunches.

When dealing with nested cavities, there are three main velocities, and therefore optical indices that must be defined and understood. Frequency (phase) velocity is the velocity of a given optical wave through a medium. Pulse (group) velocity is often defined as $\frac{d\Omega}{dk}$ within a dielectric, but is better thought of as the velocity of a group of frequencies, otherwise known as an optical pulse. Bunch (envelope) velocity is a new quantity that must now be realized for the scenario of pulse bunches. The pulses within a pulse bunch travel at the group velocity; however, one of the first observations that are made when working with nested cavities is that the cavity repetition rate tends to not follow what one would expect by simply extending the optical path length with a piece of glass. This results from the measurement of the velocity of a bunch rather than that of a single pulse. Bunches tend to travel slower than the pulses that make them up, and since an avalanche photo diode (APD) is unaware of this difference, it records the velocity of the envelop of the bunch rather than a pulse [13]. The various velocities can be described mathematically as;

$$\mathrm{v}_p = \frac{c}{n_p}, \tag{2.5}$$

$$\mathrm{v}_g = \frac{c}{n_g} = \frac{d\Omega}{dk}, \tag{2.6}$$

$$\mathrm{v}_B = \frac{c}{n_B}, \tag{2.7}$$

where v is used to represent the velocities, annotated with a subscript p for phase, g for pulse or group, and B for bunch respectively. While n_p is the phase index, n_g is the group/pulse index, and n_B is the bunch/envelop index, ω is the angular optical frequency, and k is the angular wave number. Distinction of these values is very important when dealing with tailored combs for the purposes of understanding what a given detector is monitoring or how different values in the laser characterization

should be interpreted.

With these, albeit basic, definitions, it is possible to define the repetition rates for the larger laser cavity and that for the nested FPE;

$$\nu_C = \frac{c}{2Ln_{g,C}}, \tag{2.8}$$

$$\nu_{FPE} = \frac{c}{2dn_{g,FPE}\cos\theta}, \tag{2.9}$$

where ν is the repetition rate for the laser cavity, C, or the nested FPE respectively, L is the length of the laser cavity, d is the thickness of the FPE, n_g is the group index for the laser cavity, including for the gain and the saturable absorber, and FPE receptively, and θ is the internal angle of the FPE. In practice, it would take two detectors capable of 30GHz acquisition rates to monitor both of these frequencies. The detectors available were multiple APD's capable of resolutions in the MHz range, and one 30GHz silicon detector from a company called Albis©. With this in mind, it becomes apparent that I cannot monitor the pulse repetition rates in both cases; therefore, the ν_C value is typically taken with an APD, which means that the $n_{g,C}$ in Eq. 2.8 changes to $n_{B,C}$, where the B indicates it is the index of the bunch. This small change seems almost negligible in most scenarios; however, one example of this change becoming quite significant will be discussed in Subsection 2.4.4.

In Fig.2.4, the recorded cavity repetition rates are shown as the end mirror of the laser cavity is scanned over 15mm. In part (a), we see that the repetition rate of the cavity as a whole, the blue line, decreases as the cavity is shortened, as expected. We also see something unexpected. As the larger cavity is shortened, the radio frequency (rf) associated with the repetition rate of the nested FPE, the red line, also increases. This is initially surprising since the nested cavity experiences no physical change; however, close inspection of resonance conditions of the nested cavity;

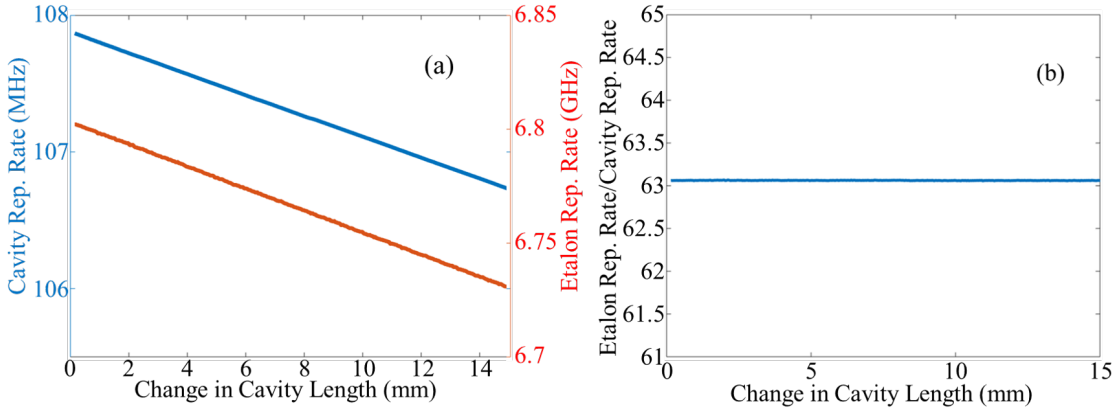

Figure 2.4: Experimental data taken from a linear Ti:Sapph nested cavity. Part (a) shows the change of a single rf peak, representing the FPE repetition rate, as the end mirror of the cavity as changed, in red. The blue line is the results of the cavity repetition rate read from a MHz frequency counter, measuring the repetition rate of the larger cavity. This shows the link between the two cavities and that alterations to one of the cavities intrinsically affects the other. In part (b), it is shown that the ratio of these two measured frequencies remains constant over the course of the scan.

$$\frac{2\omega_0 dn_{p,FPE}\cos\theta}{c} = 2N_{FPE}\pi, \tag{2.10}$$

and the larger laser cavity;

$$\frac{2\omega_0 Ln_{p,C}}{c} = 2N_C\pi, \tag{2.11}$$

and their relation,

$$dn_{p,FPE}\cos\theta = Ln_{p,C}\frac{N_{FPE}}{N_C}, \tag{2.12}$$

shed some light on this apparent paradox. Where N_{FPE} and N_C are the number of modes supported by each cavity. The two conditions in Eq. 2.10 and Eq. 2.11 must be met simultaneously in order for the laser to operate. The combined resonance condition can be seen experimentally in part (b) of Fig. 2.4, as the ratio of the two repetition rates remains constant over the entire scan. This, at first glance, seems nearly impossible, and would, practically speaking, involve at least a lot of electronics. However, whenever this has been tried in the lab, it has required only aligning the FPE angle close to normal, but not normal, and increasing the pump power by about

1 to 2 Watts. This indicates that, while the parameters of the lengths of the cavities and their phase indices cannot be easily tuned, the cavity is 'self-adjusting' via small mode perturbations, a completely passive process [13]. This is not a new discovery, as my predecessor, Dr. Masuda, was the first to observe this phenomenon, but it is a very important fact that makes these nested cavities function, and so I have stated it again here.

The relation of Eq. 2.12 shows more clearly how the number of modes within each cavity can alter themselves to lock the cavities even while the indices and lengths remain more or less static. Even more importantly, this relation shows that, via simple substitution, it becomes impossible to separate the repetition rate of one cavity from another in a nested scenario. In other words, every change made to either of the cavities, directly effects the other.

This final realization has numerous consequences, making it the arguably most important statement in this entire dissertation. Chapter 3 will show how these consequences can be used to increase sensitivity in intracavity interfereometric sensing, and Section 2.4 of this chapter will focus on the abilities these consequences lead these cavities to have.

Yet another point of interest in the time domain is the number of pulses contained within a bunch. As it turns out, this value can be controlled by the angle of the FPE and its reflectivity, which with basic alterations, the simulation discussed above can attest. It has been experimentally shown that the number of pulses per bunch also can have an effect on the behavior of the repetition rate of the cavity. The plot in Fig.2.5 clearly shows how the bunch changes with FPE angle, along with the measured cavity repetition rate, which is really a measure of the bunch repetition rate. The most interesting region to note in this particular data set is when the number of pulses per bunch decreases to only two, around 35mrad. This region seems fairly large for a set number of pulses and shows a unique positive linear

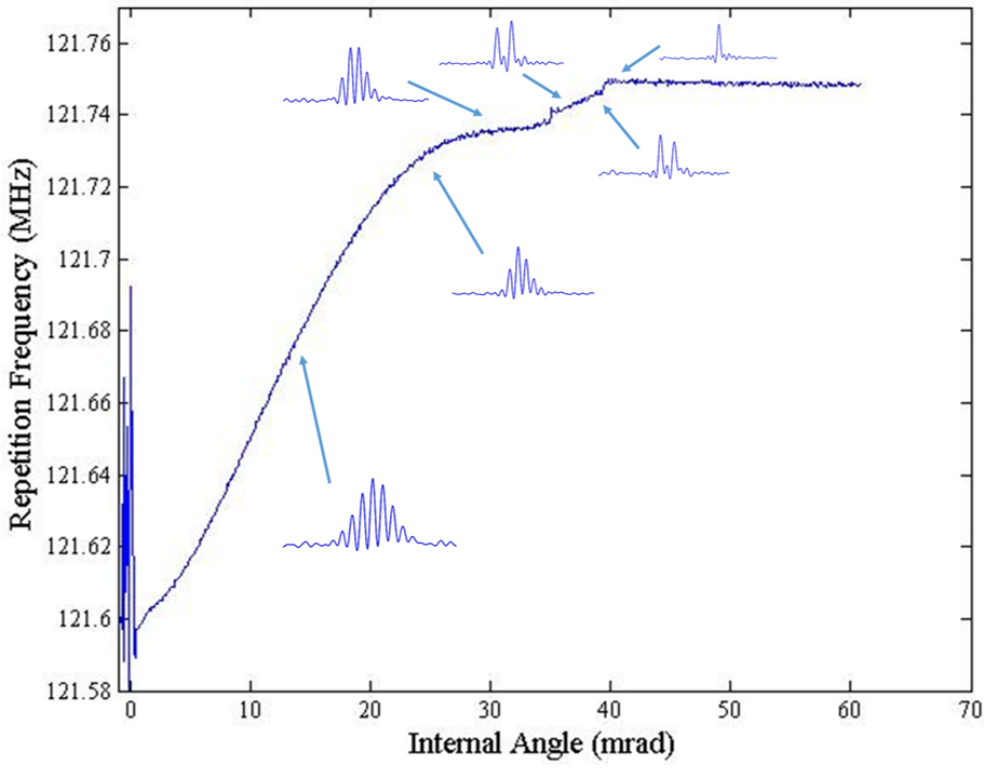

Figure 2.5: The data presented here was taken by tuning the angle of the nested FPE while the rest of the system remains static. The plotted line is the measured laser cavity repetition rate measured via a MHz frequency counter. The inlaid oscilloscope traces were taken from a GHz scope to observe the evolution of the number of pulses that exist at selected locations. There is an interesting phenomena that was first reported when this figure was first published in [13], when the cavity switches from bunch operation, to two pulses per bunch operation, and finally to single pulse operation. Here it is shown that these crucial changes in the number of pulses per bunch can be identified by a changing behavior in the laser's repetition rate.

slope that is completely unlike any other portion of this scan. It is likely that this slope change is indicative of a distinct change in cavity operation. When the cavity switches from pulse bunch operation to single pulse operation, the nested cavity goes from being a resonant nested cavity to a frequency filter. In the two pulse operation region, the cavity is in a state of transition which results in this unique slope in the measurement of the laser cavity's repetition rate. The rest of these scans' velocities can be explained by the calculations of the various cavity velocities done above.

2.3.2 Dynamics of Frequency Domain Tailored Combs

Much like what has been shown above for the time domain, the frequency domain is also modulated in a unique manner. The original frequency combs from mode-locked lasers can be described via;

$$f_N = f_{CEO} + N \times f_{\text{Rep.Rate}}, \tag{2.13}$$

where f_N is the frequency of mode N, $f_{Rep.Rate}$ is the repetition rate of the cavity that rigidly defines the frequency mode spacing, and f_{CEO} is a frequency offset from 0Hz that also defines the offset of the electric field from the pulse envelope in the mode-locked cavity [14]. f_{CEO} is known as the Carrier Envelope Offset (CEO) [15]. This *offset* can be found by extending the comb all the way to 0Hz and measuring the mismatch between 0Hz and the lowest frequency.

In the case of tailored combs, this description becomes a bit more complicated. In this modular comb regime, there are now two frequencies that define the locations of the comb teeth and their separations. There is also an offset frequency from 0Hz, but in this case, it is not the CEO, as defined above. The mathematical definition is given by;

$$f_{M,N} = f_{\text{Offset}} + M \times f_{FPE} + N \times f_P, \tag{2.14}$$

where, as before, $f_{M,N}$ is the frequency of a specific mode (M, N), f_P is the repetition rate of the *parent* cavity that rigidly defines the frequency N mode spacing, f_{FPE} is the repetition rate of the *nested* cavity that rigidly defines the frequency M mode spacing, and f_{Offset} is a frequency offset from 0Hz. A cartoon illustration of these combs is shown in Fig.2.6.

It is clear from this illustration that the tailored comb is actually the result of combining the resonances of two cavities that, when nested together, result in a frequency comb with periodic modulation. The remainder of this dissertation will

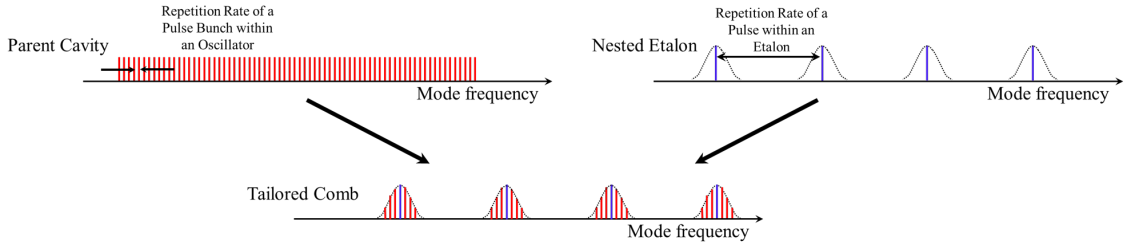

Figure 2.6: An illustration of a standard optical frequency comb with the transmission of a Fabry-Perot etalon (FPE). The upper left comb is that of a standard laser oscillator that is mode-locked. The upper right is the transmission function of the FPE. The resultant comb from the nesting of the cavities is shown below these with the elements of each of the parent combs color coded for convenience.

discuss the various ways that this new comb and its properties can be exploited to enhance measurement methods in metrology, give rise to new stabilization techniques, and used to tune to specific frequency resonances within atomic media.

Before continuing, it is worth noting that there exist certain aspects of tailored combs that have yet to be fully investigated, which will be left to the discussion of future work in the conclusion of this work. That being said, the results that have been obtained so far have provided more than enough motivation to apply these combs to certain applications and these have already produced interesting results. These results and their interpretations have been the main focus of the work presented here.

2.4 Tailored Comb Abilities

With the descriptions and definitions outlined in Section 2.3, we can now discuss the unparalleled abilities of these tailored combs. In this section, multiple methods for tailoring these combs are presented. It concludes with a brief discussion of possible applications, some of which I have already begun to investigate.

2.4.1 Precision Tailored Comb Tuning

Precision comb tuning of tailored combs was first explored by Dr. Koji Masuda in 2016. In this dissertation, I continued to investigate this topic and was able to more fully explain some of the observations as well as make some new ones. While most of the work with tailored combs has centered on the ability to view them in the rf domain, while working with Ning Hsu, we were able to partially observe the optical domain comb on a Charge Coupled Device(CCD), and the results are shown in Fig. 2.7. This was achieved by shining the laser onto a grating and then sending

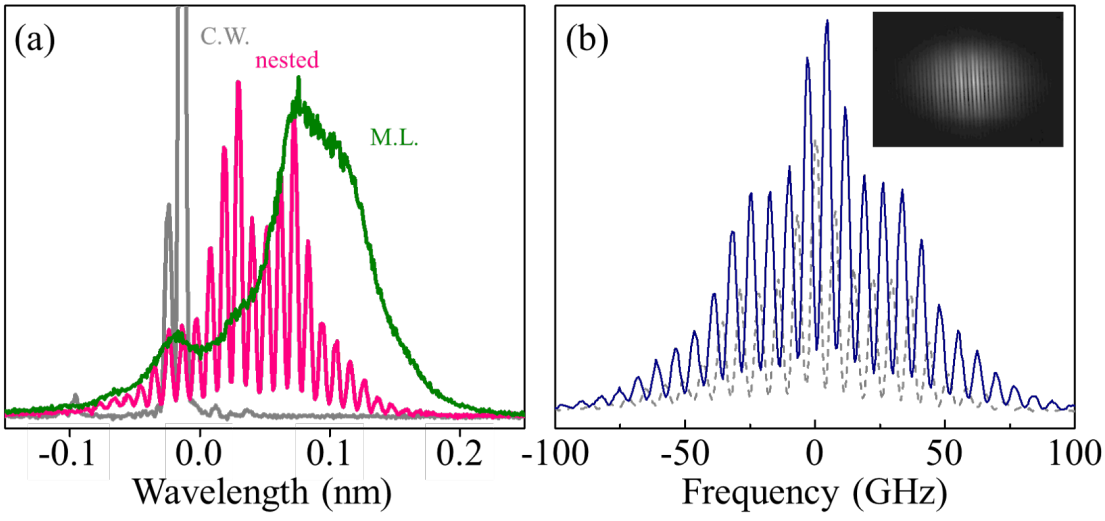

Figure 2.7: The directly observed optical spectra of the tailored comb are shown. In part (a), a plot of the same linear Ti:Sapph laser in CW operation, standard mode-locked(ML) operation, and tailored comb operation. In part (b), the nested comb is shown to shift with FPE angle, and an inset of the direct CCD image. While these plots do not show the individual comb teeth, they do resolve the GHz frequency bunch envelopes.

the beam 2-3 meters down the optical table. The MHz teeth are, sadly not observable in these plots; however, the GHz spaced comb islands could be viewed and tracked. The first experiment was to simply observe the spectra from our linear Ti:Sapph in different operations. Part(a) of fig. 2.7, we see that there is a very clear distinction, obviously, between CW and ML operation. More importantly, we see a distinction between nested cavity and standard ML. The fringe-like pattern in the nested cavity corresponds to the GHz spacing of the FPE modes, which had never before been

observed. In part (b) the angle of the FPE is tuned arbitrarily and a dramatic shift is observed. The inset in this image is taken directly off the CCD and shows the practically 100% modulation of these frequency islands. This tells us that there is no laser intensity what so ever between these FPE modes, just like the laser intensity of a frequency comb is confined to the comb teeth. What is not shown is that as we took consecutive pictures of the comb when we simultaneously observed peak ^{87}Rb fluorescences, the comb appeared identical. Thus, as the FPE angle is scanned, the comb continuously and periodically reproduces itself. This was not predicted or assumed before this data was taken.

Fig. 2.8 shows this repeating comb from the point of view of the ^{87}Rb fluorescence and illustrates the corresponding frequency shift. In part (a), the blue line shows the running average of the fluorescence as a function of FPE internal angle. The green line marks the resonance of the F=2 peak in the D1 transition [16]. The red dashed lines are the calculated modal wavelengths of the FPE that coincide with the experimentally observed peaks. The intersection of these with the green line indicate where the F=2 state is predicted to occur, which is indeed the case in this data. Part (b) is picking a specific occurrence of these fluorescences and indicating which peak corresponds to which state. This has been shown previously, but I repeated this many times throughout my dissertation research as it proves to be a very useful tool in characterizing tailored combs. The calculations to prove which state corresponds to which peak will be shown below. Part (c) is a cartoon showing a visualization of an rf comb interacting with ^{87}Rb to achieve fluorescence.

To calculate the red dashed lines, and also prove that the peaks do actually represent the states as labeled, the relation;

$$\cos(\theta) = \frac{\lambda N_{FPE}}{2n_{p,FPE}d}, \tag{2.15}$$

is used, where $n_{p,FPE}$ is 1.4534 at λ=795nm at 20^{o}C and d=15.12mm at the same temperature. This data was taken at 23.2^{o}C, and while that is a minuscule change

in d, whose number has some error to it already due to the tool used to measure it, $n_{p,FPE}$ changes $1\times10^{-5}/^{o}$C. With these changes, it is possible, as shown, to predict the location of ^{87}Rb D1 transition fluorescence peaks accurately and to prove that the states are as marked. This shouldn't be overly surprising for two reasons. First, the FPE scans the laser wavelengths from low frequencies to higher ones in this setup, so it makes sense that the F=2 state would come after the F=1. Secondly In the notes of Dr. Daniel Steck [16], it is stated that the F=2 state has a higher coupling, meaning that it is likely to have a higher amplitude in fluorescence, which this data clearly shows to be the case.

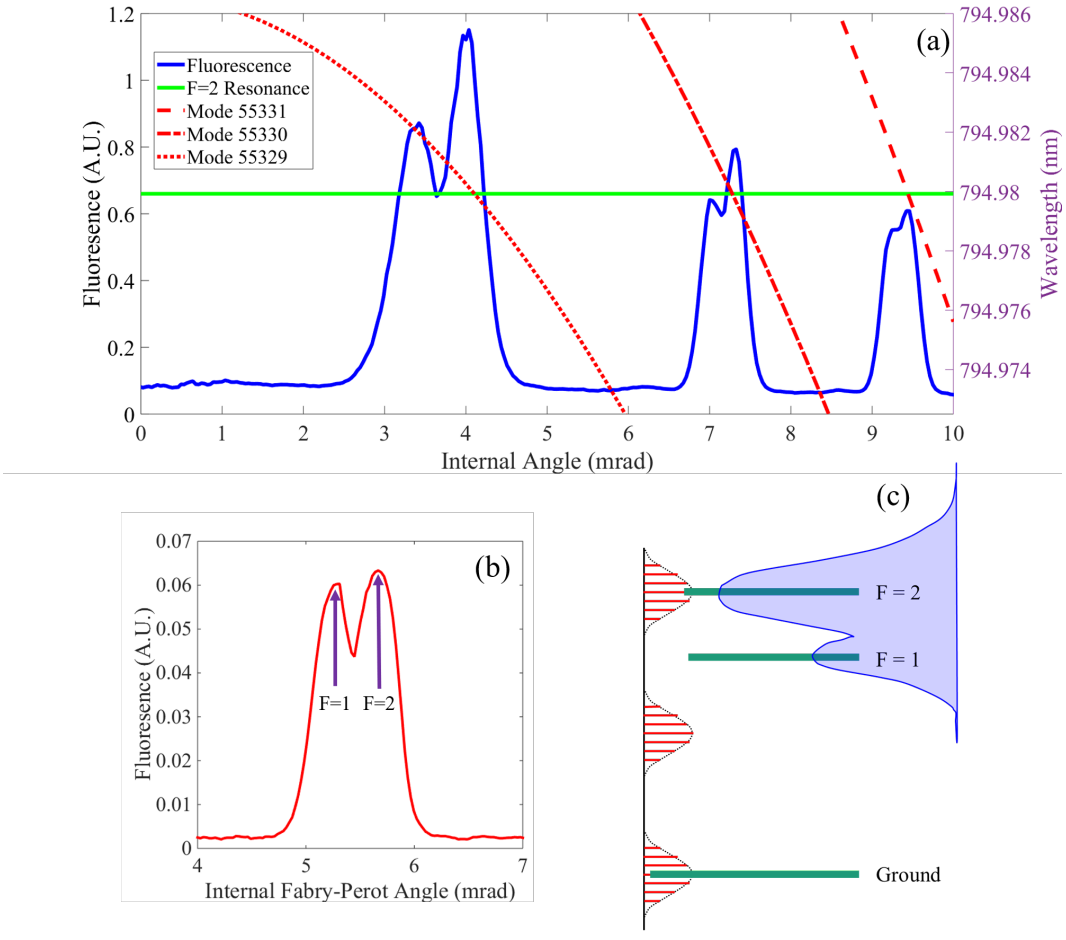

Figure 2.8: A demonstration of the predictability of the mode tuning of nested cavities. Part (a) shows how the central wavelength of the FPE modes as they are scanned over the ^{87}Rb resonances. The green line marks out the F=2 resonance of the D1 transition and the red dashed lines coincide with the peaks of the measured fluorescence signal. Part (b) is a zoomed in version of the first resonance in part a with the peaks labeled and part (c) is a cartoon of how the frequency bunches scan over the labeled resonances.

With multiple evidences all in agreement, it is reasonable to conclude that we not only can accurately state which peaks we are observing, but also predict the FPE internal angle at which they will appear and which FPE mode number is in resonance. Therefore, this ability to use the nested cavity scenario to predictably and accurately align to D1 ^{87}Rb resonances proves the precision with which these tailored combs may be tuned.

2.4.2 Nested Cavity Coupling

As discussed in Subsection 2.3.1, the nested cavity scenario results in a unique coupling of cavity characteristics. The repetition rate of the laser cavity and that of the FPE are coupled via;

$$\mathcal{R} = \frac{\nu_{FPE}}{\nu_C} = \frac{n_{B,C} n_{p,FPE}}{n_{p,C} n_{g,FPE}} \frac{N_C}{N_{FPE}}. \tag{2.16}$$

It is important to notice here that it is the bunch index that is used for the laser cavity, rather than that of the group. This is indicated here because in practice, as previously stated, the APD used to measure the cavity repetition rate cannot distinguish individual pulses within a bunch. This results in data that shows the repetition rate of a bunch in the larger cavity and the repetition rate of individual pulses within the nested cavity. This point, while negligible in most circumstances, will be discussed in detail in Subsection 2.4.4.

As has been discussed multiple times, when looking at the data taken in lab, we see that the ratio of the Fabry-Perot repetition rate, ν_{FPE}, to the *parent* repetition rate, ν_C, leads to an integer, I, plus a small fractional offset, δ. This is interesting since there is nothing from Eq. 2.16 to suggest a result that is an integer.

$$\mathcal{R} = I + \delta. \tag{2.17}$$

We have seen that the frequency tooth chosen to represent ν_{FPE} can change the value of I, but leaves the value of δ unaffected. It has also been observed that the scanning of the parent cavity length has no measurable affect on δ, but that changing the FP angle does as shown in Fig. 2.9. This latter tuning shows that δ has an inverse relationship with the etalon internal angle. To ease comprehension, we can separate δ into two components that can be uniquely separated by these two cavity manipulations. Δ will be used to define the variance of δ and $\bar{\delta}$ will describe average the value. Henceforth, we will call δ the tuning parameter. From this analysis, it can be said that the variance, Δ, can be used to describe the noise, or motion, of the tailored comb, and $\bar{\delta}$ indicates the value of comb detuning from the case where

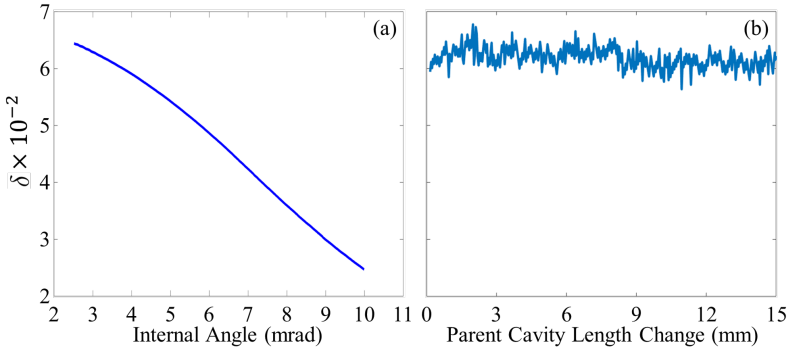

Figure 2.9: This figure shows the tuning factor, δ, as the internal angle of the etalon is changed (a) and the cavity length is changed (b). From this figure, we see that over the course of about 8mrad, $\bar{\delta}$ changes by 4×10^{-2}, where we see this value unchanged in the cavity length change. In the cavity length scan, we see a Δ value of about 0.25×10^{-2}. This draws two conclusions, first, we can calculate the angular tuning of $\bar{\delta}$ as $\delta \times \nu_P$ which is about 4.24MHz in our system where the variance, $\Delta \times \nu_P$, amounts to around 265kHz. Keep in mind these are unstabilized values, but that the tuning versus the stability are already separated by an order of magnitude.

f_P is a sub-multiple of ν_{FPE}. Since our observations show that these parameters can be independently manipulated, it is reasonable to assume that there exist the ingredients for independent comb tuning and stabilization, something that has not before been realized by other stabilization techniques. The remainder of this report is to propose a comb stabilization strategy that could drastically reduce the amount of effort necessary to create a stationary frequency reference.

Another result of the definitions given in Eq. 2.16 and Eq. 2.17 is a clearer understanding of the comb structure as defined by Eq. 2.14. The logic follows as;

$$\mathcal{R} = \frac{\nu_{FPE}}{\nu_P} = I + \delta \tag{2.18}$$

$$\nu_{FPE} = \nu_P I + \nu_P \delta. \tag{2.19}$$

With this new definition, Eq. 2.14 can now be written only in terms of the parent cavity repetition rate;

$$\nu_{M,N} = \nu_{\text{Offset}} + M \times (\nu_P I + \nu_P \delta) + N \times \nu_P. \tag{2.20}$$

Finally, this clarification of the mode structure leads to an important realization in the spacing between frequency islands within an rf comb. Namely;

$$\nu_{M+1} - \nu_M = \nu_P I + \nu_P \delta, \tag{2.21}$$

which clearly shows that as δ is tuned, there is a clear effect that is measurable across the entire rf comb.

Proposal of stabilization method

The ingredients defined in the previous section will now be used to propose a stabilization system that does not require spectral broadening, f to $2f$ comparison, or really any comb manipulation outside the original oscillator. Here we are defining a stable comb to be one in which the value of Δ is minimized, which is to say that the noise, or motion, of the comb with respect to itself is at a minimum, or negligible value. Decreasing all motion of the comb would require the optical frequency of the comb to be locked to a reference, which is possible here and will be discussed at the end of this section. As shown in Fig. 2.9, Δ was not affected by angle tuning and $\bar{\delta}$ was found to be equally independent of the parent cavity length. If the tuning parameter is easily measurable using the accessible rf that makes up a tailored comb, then there is no need to manipulate the comb further after the oscillator to achieve a stationary comb. In fact, all that is required is to clamp the variance as much as possible.

This simple suggestion actually reduces the amount of effort for a stationary comb immensely, since all previous schemes require complicated frequency broadening and comb interference techniques to accomplish stationary status. In fact, most labs require frequency standards of institutions like the National Institute of Standards and Technology (NIST) since the cost of such a scheme is prohibitive. While such a reduction in physical footprint and economic burden are already enough to qualify this as a marked achievement in frequency comb science, we have neglected to discuss

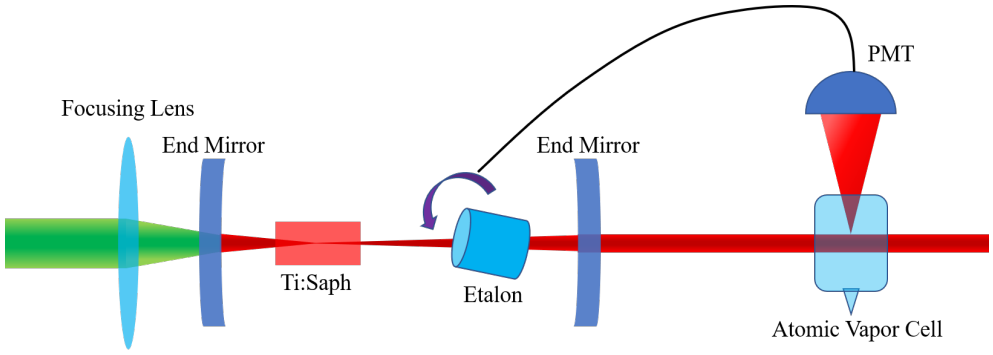

Figure 2.10: A basic schematic is shown to indicate where aforementioned detectors and references would be located in reference to the original cavity as well as the elements that these detectors would control. A Photo-Multiplier Tube (PMT) monitors the fluorescence of an atomic vapor cell. The maximum of this fluorescence is used to stabilize the angle of the FPE.

the abilities of tuning $\bar{\delta}$.

Remembering that $\bar{\delta}$ is the comb detuning from the case where the frequency ratio, Eq 2.17, is equal to a perfect integer, I, we see that this value can be used to actually tune the comb teeth values without affecting the stabilization, that is the value of the variance, Δ. This is an idea that cannot exist in the case of a regular frequency comb as all the parameters of the oscillator are interconnected in that case. This results in the ability to control the laser frequency, either by locking it to an atomic transition or simply scanning it over a predetermined range, without the worry of destabilizing the comb. In many of the original comb stabilizing schemes, it was also desired to lock the optical frequency to a reference. In this proposed method, that is possible again. When the angle of the etalon is tuned within the cavity, the optical frequency is tuned, as shown in previous sections. It is possible to lock the tailored comb to the peak of an atomic transition via a feedback loop where the angle of the FPE is dithered to maintain a maximum fluorescence from a reference vapor cell. This would create a completely stabilized and locked comb source. It is, perhaps, more interesting that as this comb optical frequency is tuned, the comb remains locked, and therefore stabilized to itself.

This creates a highly stable, tunable source capable of a large tuning range and adjustable spectral width (based on pulse width) at the efficiency level and cost of a typical mode-locked oscillator. A basic schematic of the implementation of this proposal is shown in Fig. 2.10.

In this subsection it has been shown that by analyzing the frequency elements of a tailored comb, it is possible to achieve comb stabilization without femto-second pulses or f to $2f$ comparisons. More than that, it is also possible to achieve a significant frequency tuning range that is independent of this stabilization, or use traditional frequency locking methods. This proposed method makes it possible to stabilize a laser cavity whose spectral width spans only a few GHz rather than a full octave, since it only requires the monitoring of easily accessible rf elements that make up the tailored frequency comb. This requirement is found simply by the fact that only two frequency islands within a nested comb are required for the necessary frequency ratio to be measured. Realization of this scheme could result in a simple and cost effective method for stabilizing comb sources for the price of a simple mode-locked cavity.

2.4.3 Tailored Comb Stabilization

While the cavities used throughout this dissertation are not actively stabilized, no description of a new type of frequency comb would be complete without some discussion the comb's stability. In this subsection, I provide a brief comparison of cavity frequency stabilities of standard cavities at similar powers to nested cavities in both pulse bunch and single pulse operation. These observations have never been conducted for a tailored comb before this dissertation. The calculations presented here are standard Allan deviations. Descriptions of the methods can be found in Appendix A.2. Also, importantly, τ and Time in all these plots are given in hours, contrary to the typically Allan deviation plots where they are typically in seconds.

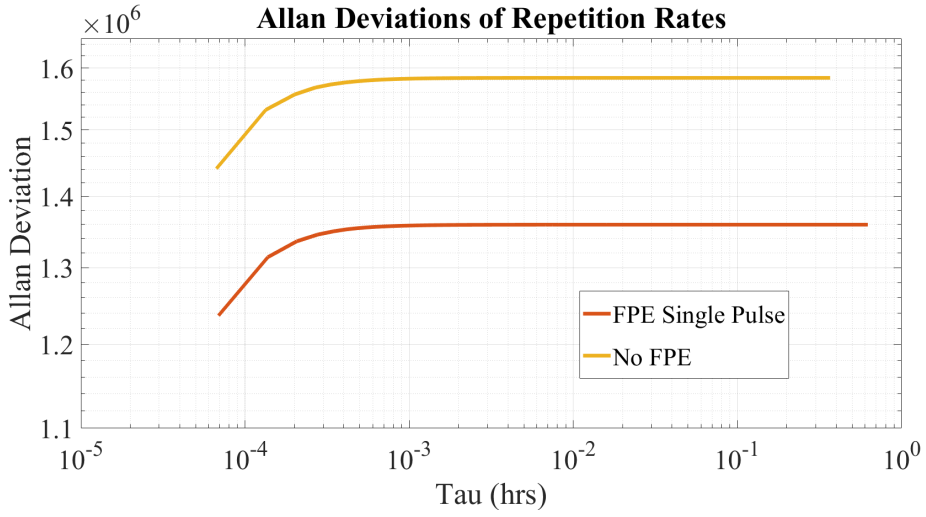

Figure 2.11: The data presented here was all taken from the same cavity at similar pump powers in the same day. This data is taken via an APD and a frequency counter. Therefore, this data shows the Allan deviation of the repetition frequency in the laser, which is the pulse leading edge repetition rate. The Allan deviations for various cavity operations are shown as indicated by the legend.

The results of the measurements of the Allan Deviation for various cavity operations are shown in Fig. 2.11. Since these cavities were not actively stabilized, the characteristic minimum of the Allan deviation can not be accessed with the equipment available in our lab. However, there are clear separations between the various types of cavities.

Allan deviations are a measure of the instability of a frequency for a period of time. The higher the value, the less stable the frequency that is being observed. For Fig. 2.11 we see that the least stable scenario for the measured cavity repetition rate is that of the bare cavity with no nested FPE. This is more or less expected as the nesting of a resonant FPE within a cavity for two unstabilized cavities to be locked together. Even though two unstabilized cavities do not create a super stable situation, it is reasonable to assume that this would be more stable than no locking what so ever.

An interesting result from this data is that the case of single pulse oscillation in the presence of the FPE is more stable than that of the pulse bunch. This may be

due to the fact that the sidebands in the frequency domain associated with pulse bunching are now forced to overlap with other frequency bunches, as detailed in Fig. 2.6. This creates another degree of locking together that is not present in the bunching scenario, since the sidebands in that case do not interact and thus their spacing in reference to adjacent frequency groups is not locked. This changes for the single pulse operation in that the comb must maintain equal spacing and so these sidebands are now forced to overlap with each other.

It should be noted that the Allan deviations reported here are all of the same order of magnitude and so this separation observed between the various laser operations is considered quite small, although, in caparison to a stabilized Ti:Sapph oscillator, the deviations here are very large. Current research into comb stabilization can reach values as low as 10^{-18} for a stabilized Ti:Sapph cavities [17]. Obviously, we are nowhere near this value.

If we do a similar analysis with a 13GHz rf spectrum analyzer and a 30GHz detector, a similar result can be achieved. Combining these with the results from the frequency counter, we can take the frequency ratios whose Allan deviations are shown in Fig. 2.12. Notice that these values are below one, showing significant stabilization between the frequency components of these two cavities. This result is low enough to classify these frequencies as stabilized together, even though, individually, their values are noisy.

The data presented in Fig. 2.12 was chosen due to the fact that the standard deviations of the frequency over the total time of observation varied by 50% or less for each mode of operation, and so the results are considered reliable for those pertaining to the frequency counter. In some data the standard deviations varied by more than this amount for different modes of operation, and so are not used to draw conclusions about the laser stability individually.

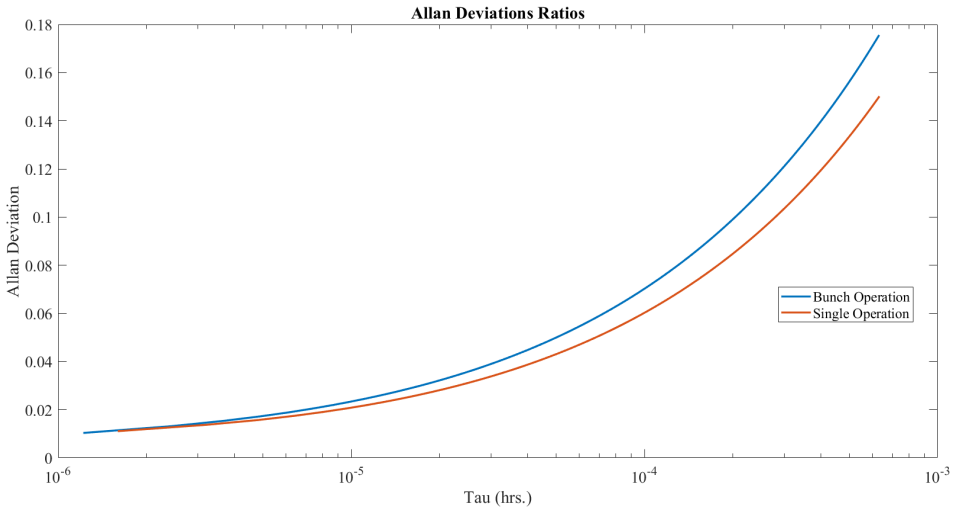

Figure 2.12: Allan deviations are shown for various frequency ratios for both single pulse and pulse bunch cavity operations with the FPE in place. The blue line is for pulse bunch operation and the red line is for the single pulse operation with nested FPE.

Two important noteworthy points arise from this. First, the spectrum analyzer, while faster than the frequency counter, is much less stable. Second, even with these variance in the standard deviation measurements from the spectrum analyzer, the frequency ratios were found to be orders of magnitude more stable than their individual frequency counterparts. This is an indication of passive comb stabilization without the fixing of the Carrier Envelop Offset (CEO) of the comb. To the best of my knowledge, stabilization of frequency combs through passive methods has never been reported in this manner before. CEO stabilization has been achieved passively via Difference Frequency Generation (DFG) [18] and also for Optical Parametric Oscillators pumped by unstabilized Ti:Sapphs [19]; however, neither of these methods are comparable to what is presented here. Their focus on the CEO is an inherently different type of stabilization, and they only needed to worry about a single comb frequency whereas the tailored frequency comb utilizes two.

2.4.4 Tailored Comb Metrology

One intriguing application that has arisen from investigations of nested combs has been the measurement of the linear refractive index of the nested FPE. To motivate this concept, we return to Eq. 2.16, which describes the frequency ratio. This ratio can be directly tied to the linear phase index of the nested FPE. The linear phase index is important for two reasons. First, the phase index is nearly impossible to measure without taking into account the length change of the sample. Secondly, many minute phenomena can be indirectly observed via minuscule changes to this index. As will be shown, and has also been written about by Dr. Koji Masuda [13], the length of the FPE can be dropped out of the calculation of the phase index using this method. As far as minuscule changes to phase index, our group spent multiple years in a collaboration that investigated crystal structure damage due to neutron radiation [20]. One major finding of this dissertation is the invalidation of these previous results as well the discovery of issues that have severely hampered this particular project, though the results presented in this chapter and this section indicate that future methods will prove much more successful.

Before discussing these latest revelations, it is helpful to review the theory that originally motivated this work. This mathematical result comes from taking the ratio of the frequency ratio for two different laser setups, or, more clearly, ratio of some initial reference to an instance where the phase index of the FPE has been altered. This is called the *super ratio* and is defined, without simplification, as;

$$\mathfrak{R} = \frac{\mathcal{R}_0^{-1}}{\mathcal{R}_1^{-1}} = \frac{\frac{\nu_{C,0}}{\nu_{FPE,0}}}{\frac{\nu_{C,1}}{\nu_{FPE,1}}} = \frac{\frac{n_{p,C,0}n_{g,FPE,0}}{n_{B,C,0}n_{p,FPE,0}}\frac{N_{FPE,0}}{N_{C,0}}}{\frac{n_{p,C,1}n_{g,FPE,1}}{n_{B,C,1}n_{p,FPE,1}}\frac{N_{FPE,1}}{N_{C,1}}}. \tag{2.22}$$

It has been discussed at length within our group, and agreed, that most of this equation remains constant in both scenarios, the ratios of the mode numbers as well as the ratio of the group indices remain constant and so cancel out. This simplifies Eq. 2.22 to;

$$\mathfrak{R} = 1 + \frac{\Delta n_{p,FPE}}{n_{p,FPE,0}}, \tag{2.23}$$

where $\Delta n_{p,FPE}$ is the change in the refractive index of the FPE. This is accomplished by assuming that, for small index changes, the ratio of modes, group indices, and the larger cavity effective phase index would all experience negligible changes, and thus drop out.

This equation, from its simplicity, would seem very easy to prove, but that turns out not to be the case. A paper was published quickly on this result with regards to nuclear damage to crystal structure before it could be tested on a more well known scenario [20]. Since 2014, I have, with many different lab mates and professors, including many from the original publication, attempted to verify the reported results and prove the stability and repeatability of this technique. The remainder of this subsection is devoted to all of the work we have all put into this project and our findings.

When I first joined this project, in the Fall of 2014, I wanted to do a simple test of this mathematical result. I was going to wrap a heating coil around a nested FPE and complete a controlled experiment to monitor how the frequency ratio changes with applied temperature. The results were so clear that they were accepted for an oral presentation at the Conference on Laser and Electro Optics(CLEO) 2015 [21] and are shown in Fig. 2.13. It was not until I was preparing a manuscript for publication that I noticed the data had some abnormalities. First, the theoretical prediction is linear for the change in phase index on this scale, where the experimental data shows some nonlinear curve at its lowest values. Secondly, there were only four points here, and when more are added, the fit is worse. Finally, while these points appear to mostly match this predicted value, there is no assurance about the central wavelength of the laser, which is an important aspect of phase index.

To address these main issues, I embarked on a multi-year project to better understand this frequency ratio, which is, ironically, how the majority of the preceding chapter came into being. After many different trials and investigations, a number of

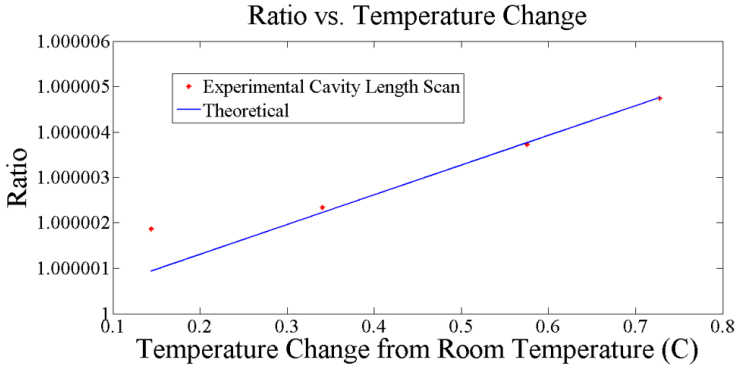

Figure 2.13: Temperature dependent ratio of ratios results, first presented at CLEO 2015. The red points are the result of the average ratio scanning the length of the larger laser cavity four times. The blue line corresponds to the expected theoretical result assuming the Thermal Index Coefficient for fused silica is $\alpha_T = dn/dT = 1.2 \times 10^{-5} \frac{1}{^oC}$.

important realizations have been discovered and some of the latest results are shown in Fig. 2.14.

The first change from this initial data was to no longer use a cavity length scan, but rather to follow the wavelength of the FPE modes instead. This solves two problems. First, there was always some question of repeatability in all scans using mechanical stepper motors resulting from the slippage of the screw. This means that the cavity length scans may not have always been in the same place. Secondly, by utilizing the angular scans, and using ^{87}Rb as a reference, we could ensure that all data were always analyzed at exactly the same wavelength. In Fig. 2.14 part (a), the results of taking only the same wavelength is shown along with a linear fitting.

One oddity from these new methods has been that the slope was always negative, even though it is well known that the index should move in a positive direction in fused silica. Even more striking, these ratio calculations have never been able to accurately replicate the accepted value of dn/dT for fused silica, $1.28 \times 10^{-5} \frac{1}{^oC}$. Calcium fluoride was also investigated. Its dn/dT has the opposite sign than that of fused silica at a wavelength of around 800nm. The experimental results again gave a negative slope and could not reproduce the value of dn/dT.

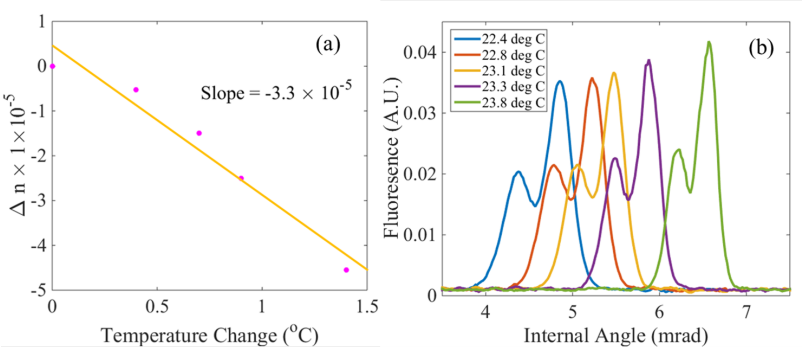

Figure 2.14: Data plots showing that changes to the refractive index due to applied heat can be clearly seen both in the frequency ratio as well as in the angular location of ^{87}Rb fluorescence. The Δn in the y-axis of part (a) is calculated via Eq. 2.23. It is important to note that fused silica is known to have a refractive index thermal coefficient of $6 \times 10^{-6} \frac{1}{^{o}C}$. If the data here were to agree with this number, the slope would be positive and less steep. Part (b) shows how the ^{87}Rb fluorescence occurs at different internal FPE angles for different applied temperatures. This is expected and, possibly, a more explicit way to determine refractive index.

From this perplexing result, I then moved to part (b) of Fig. 2.14. Using the location of the F=2 peak for each temperature, I calculated the necessary change in refractive index, assuming that the change in thickness, which is known to be a full order of magnitude less, was negligible. The results of this are shown in Fig. 2.15. This calculation is done using the F=2 peak locations of Fig. 2.14 part (b) to solve Eq. 2.15 for $n_{p,FPE}$, where d, N and λ are considered constant. This results in a slope that is very close to the well known value, making this technique a very accurate method for calculating refractive index.

While the super ratio is still not completely understood, as evidenced from the experimental data, it is clearly affected by changes in the linear refractive index. Suggested corrections to Eq. 2.23 have been to take into account the group index changes for the FPE, although these are quite small, or to try and account for index changes in the larger cavity as a whole, which is quite difficult to predict. So far, none of these corrections have yielded results close to the accepted value. As evidenced by

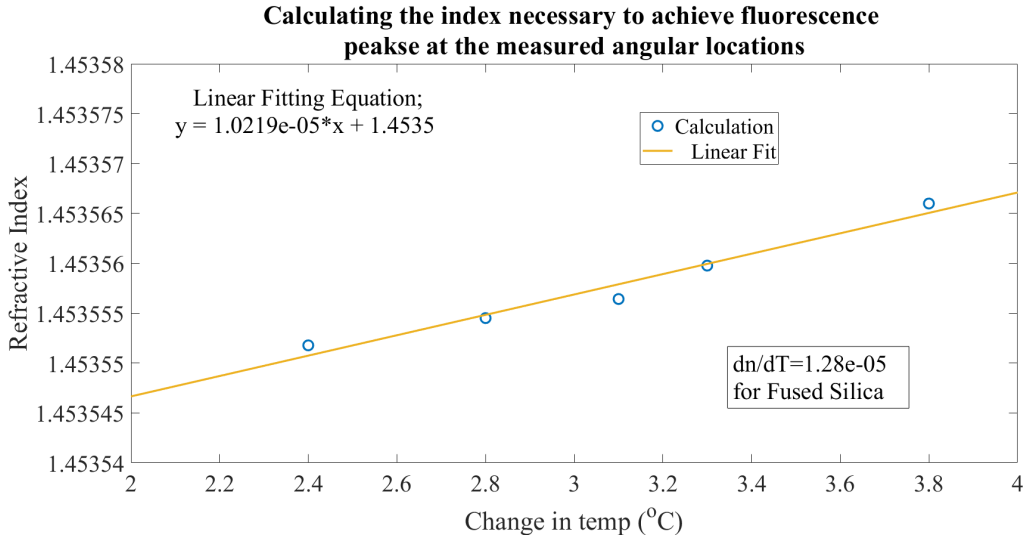

Figure 2.15: The data shown here was calculated from the peaks in Fig. 2.14 part (b) using Eq. 2.15. The results are shown in the blue line and markers. The yellow line is the linear fit of this data. The slope represents a calculation of dn/dT for the sample, fused silica. The fitting equation is shown in the upper inset box of the figure. The accepted value of dn/dT for this sample is 1.28×10^{-5}, which is very close to the calculated slope. The y-offset represents the refractive index at 0^oC temp change, which is 20^oC for this set. This value for fused silica, for a wavelength of 795nm, is 1.4534, which is very close to the value in the fit equation.

the dn/dT calculations using only the fluorescence peaks, the mode numbers, or at least those referenced for the FPE, can remain unchanged. This has not been proven out right for the larger cavity, though an argument can be made in two ways. First, in Subsection 2.4.2, it is shown that the modes of the two cavities are coupled so if one changes, or does not change, the other should follow. Second, if the fluorescence peaks in Fig. 2.14 part (b) are the result of scanning an entire frequency group over the F=2 state, then the peak fluorescence should be the center of the frequency group, which would imply that this peak does not occur on a larger cavity side band.

Another important point to remember is the method used to measure the frequency ratio. That is that an rf peak to represent the FPE repetition rate must be chosen correctly on the spectrum analyzer, which is fed by a 30GHz detector. A few different methods have been tried for this, the favorite being the calculation of the repetition rate of the FPE from its thickness and choosing an rf peak closest to that value. This

is almost always a clear choice based on this method. In terms of the repetition rate of the larger cavity, as stated previously, an APD is used in conjunction an rf frequency counter. While the 30GHz detector can be said to measure the rate of an individual pulse in the FPE, the counter with the FPE is measuring the leading edge of the pulse bunch. While this value has been confirmed on the spectrum analyzer, this confirmation only justifies using the leading edge. The point remains that in one case a *pulse* velocity is measured, and in the other the *bunch* velocity is recorded. This leads to a question of whether or not this is truly the frequency ratio described in Eq. 2.16, or is it something different. If it is something different, it is possible that the ratio that is the basis of this metrology may not be able to be accurately measured. There is the added issue that a theoretical modeling of the bunch velocity has not been done.

While this dissertation presents a true measurement of the linear refractive index of an FPE to an incredible level, the frequency ratio, which would ideally remove uncertainties due to FPE thickness, has yet to yield accurate results. More work must be done before this method can be trusted and more widely published; however, the recent discoveries of the comb ratio stability and the curve in Fig. 2.15 are very promising for the future of this technique.

In order to solve these problems with the frequency ratio measurement, it is necessary to purchase new and faster equipment in the lab. Specifically, the use of two, rather than one, 30GHz detectors and a scope capable of at least 12GHz resolution. This would allow us to measure the pulses bunches in the time domain, such that an individual pulse within a bunch could be tracked while simultaneously using the rf spectrum analyzer to measure the rf comb. Being able to measure pulse velocities in both domains at the same time would yield a much more accurate value for the frequency ratio and would solve the issue of comparing bunch characteristics to pulse characteristics.

2.5 Conclusion

This chapter has served as a summary of the knowledge of nested cavities and their resultant tailored combs. These cavities and structures have proven uniquely interesting and generated a lot of questions, many of which I hope have been answered in this chapter, though definitely not all. This topic requires more in-depth study in multiple facets pertaining mostly to finer resolution observations of the time and frequency domain characteristics, as well as closer investigations into stability and applicability to wider applications.

Other characterization methods should be conducted, such as resolving the MHz teeth via an optical spectrometer. This, of course, requires the construction of a very large spectrometer. Another option would be to create a smaller laser cavity with a much faster repetition rate and attempt to nest an even smaller etalon inside so that a smaller spectrometer is required. It would also be interesting to look at an auto-correlation that encompassed more than three pulses. This may also require some new methods of interpretation as this is a comparison of outer pulses to the central pulse rather than each pulse to itself. With this in mind, it would also be preferable to obtain a higher resolution image of the pulse bunch in time, which requires a much faster oscilloscope.

Aside from these future observations, there are also a few interesting studies that I believe are motivated by the work presented here. The first of these would be to conduct 2-photon absorption measurements in ^{87}Rb to see if tailored combs can resolve the hyperfine structure of atomic states. This ability would, depending on its resolution and success, could lead to better atomic state imaging and preparation, and well as small magnetic field detection. Another study which already has preliminary data presented in Subsection 2.4.2, would be to look at the ability to stabilize a large mode-locked cavity simply by stabilizing a nested FPE. This ability would allow scientists to construct much more complex cavities for frequency references

in less controlled environments because they would be easier to stabilize. If this were achieved, it could be a major advancement in frequency comb metrology and referencing. Finally, perhaps a more obvious question would be: now that we have studied the nesting of a single cavity, what are the limitations to the number of cavities it is possible to nest and how are dynamics, pulse trains, and comb structures effected with the increased number of nested cavities. Each of these studies could yield very interesting results and possibly increase the interest in these unique comb structures.

With the completion of the preliminary characterizations and studies presented in this chapter, I hope that I have sufficiently motivated the utility and dynamic modular nature of these comb structures and cavities, as well as addressed some of their limitations and drawbacks. In the future, I expect that these cavities may be used for many different applications, including atomic imaging and state preparation, stabilization methods, high repetition rate mode-locking, and spectroscopy using GHz combs with MHz side-bands for added precision. The versatility and ease with which these cavities can be designed will likely prove invaluable in these future applications.

Chapter 3

Intracavity Phase Interferometry and Resonant Dispersion

3.1 A Brief Introduction to Intracavity Phase Interferometry

Intracavity Phase Interferometry (IPI) is a frequency comb metrology technique in which two mode-locked pulses are generated within the same cavity, thus making them initially identical. As these twin pulses oscillate, a sensing element in the cavity imparts different phases to each intracavity pulse, which, due to the fact that this is an active cavity environment, alters the comb frequency. The measurement is conducted by beating these two combs together outside the cavity, and the resultant beat-note can be used to directly calculate this phase difference [22]. In this chapter, IPI will be fully introduced and a novel enhancement method will be shown with experimental data for a proof of concept as well as the first observation of actual sensitivity enhancement.

3.1.1 Defining Intracavity Phase Interferometry

As already stated, IPI involves generating two combs from a single cavity, and then measuring the offset between these two. The offset of these combs is generated by a phase difference. This phase difference amounts to a frequency difference since this occurs in a active cavity environment via;

$$\Delta\omega = \frac{\Delta\phi}{\tau_{RT}} = \omega\frac{\Delta P}{P}, \tag{3.1}$$

where $\Delta\omega$ is the measured beat-note, $\Delta\phi$ is the overall phase difference between the two pulses, and τ_{RT} is the round trip time of the cavity. This imparted phase difference can also be seen as an apparent change in cavity perimeter, which is described mathematically after the second equals sign in Eq. 3.1. Here, ω is the average optical pulse frequency, ΔP is the apparent change in cavity perimeter, and P is the initial perimeter of the cavity.

IPI has many advantages over other comb sensing methods. First, it is independent of amplitude noise. The measured beat-note is completely described by a shifting of two relative combs, which means that the amplitude of the pulses measured at the location of the detector is not taken into account. This also implies that the cavity output power can be relatively low, but still allow for accurate measurements to be taken. Another advantage is that mechanical noise is completely washed out. This is because the pulses are generated by the same cavity, meaning that all phases imparted to one pulse are automatically given to the other, except for the sensing element, which is specifically designed to give a different phase to each pulse. Finally, unlike in other comb metrology, stabilization of the carrier envelop offset (CEO) of the combs is completely unnecessary. In fact, the differential phase shift imparted by the sensing element is translated into a shift of the CEO, which is precisely what IPI is measuring.

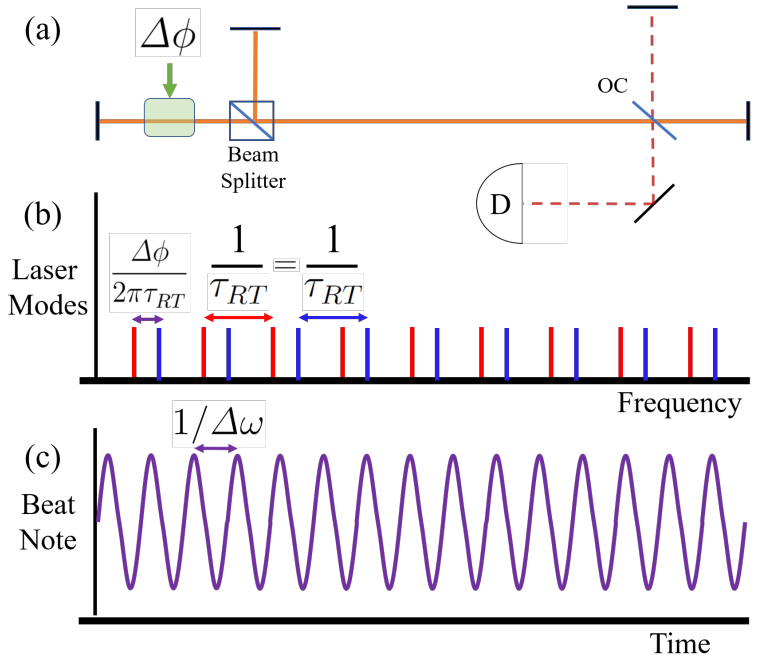

Figure 3.1: This cartoon is included to explain the technique of Intracavity Phase Interferometry (IPI). In part (a), a simple linear cavity diagram of an IPI sensor is presented. The solid red lines indicate beam paths within the cavity while the dashed indicate paths outside. A beam splitter is used to split one side of the cavity into two arms, a reference and sample arm respectively, where the sample arm has a differential phase element, in green, labeled $\Delta\phi$. An output coupler (OC) is located at the other end of the cavity to extract the pulses into a delay line, which overlaps them in time on a detector (D). Part (b) is a frequency domain illustration of the two combs, red and blue, associated with the two pulses oscillating in the cavity of part (a). As indicated, the two combs have the same repetition rate, though they are offset in frequency due to the phase shift, $\Delta\phi$. Finally, part (c) shows the output of detector D in part (a) which is a beat-note signal of frequency $\Delta\omega$ corresponding to the separation of the combs in part (b) due to the phase shift $\Delta\phi$.

An illustration of the IPI technique is shown in Fig. 3.1 to provide clarity to the descriptions presented above. In part (a), a simple linear cavity is shown where the solid red lines indicate beams within the cavity and the dashed ones indicate beams outside. The beam splitter within the cavity separates one end into reference and sample arms, where the sample arm has an added phase element indicated by a green box and labeled with a $\Delta\phi$. An output coupler (OC) is then used to extract the two pulses into a delay line to overlap them in time on a detector (D). Part (b) of this figure is a frequency domain picture of the effect of the phase element in the sample

arm. The comb teeth of the two pulses are represented by two different colors, red and blue. The separation of these combs is labeled by the phase shift that causes it, $\Delta\phi$, and the separation of the teeth in each individual comb is shown to be equal, since both combs are generated by the same cavity. Finally, part (c) is a drawing of an ideal beat-note signal, $\Delta\omega$, resulting from the beating of the two combs shown in part (b).

3.1.2 History of Intracavity Phase Interferometry

IPI is by no means a new technique. The research group of Dr. Jean-Claude Diels invented this technique and has been investigating it ever since [23][24] [25][26][27]. Throughout this extensive work, many important advances and realizations of this technique have been made almost exclusively from this group.

Since the first article publication in 1991 [28], multiple aspects of IPI have been studied. Kerr lens mode-locking was investigated as a possible way of generating bi-directional pulses [29]. Though ring lasers are the cavity of choice, since the beginning, linear lasers have also been successfully utilized and compared to their ring counterparts [30][31]. The cavity stabilization's effect on the precision of this technique was then studied in the early 2000's [32]. Outside of standard laser cavities, optical parametric oscillators (OPO) have also successfully been demonstrated in IPI experiments starting in 2010 [33][34].

With all these aspects to investigate and understand, there have been almost as many applications. IPI has been used as a measure of nonlinear index by varying pulse intensities in nonlinear media within a cavity [33]. It has also been used in magnetic experiments by monitoring Faraday phase effects in crystals [35]. This magnetic sensing has even lead to greater application variety in the detection of ground water via highly sensitive magnetic measurements [36]. Finally, perhaps the most obvious

application, and the one that was utilized in the work of this dissertation, is that of a gyroscope, where the pulses' phase difference is generated by spinning the generating cavity [30] or simulating such rotation [37].

While IPI's brief history has been contained mostly to one research group in the South Western United States, the numerous publications, advances and applications show just how important and serious the results of these studies have been, not to mention the three patents awarded specifically to this topic [38][39][40]. As of early 2019, yet another patent has been issued on IPI, specifically having to do with the research contained within this chapter [41]. IPI's incredible sensitivity has an ever growing interest in the optical community, and, hopefully, the latest advancements that are outlined in the rest of this chapter will motivate this increasing curiosity.

3.1.3 Designing Intracavity Phase Interferometric Sensors

This subsection will focus on only those specific elements that take a standard mode-locked laser cavity, and turn it into one of the most sensitive optical metrology devices.

Obviously, since this is a *frequency comb* based technique, we need to start with a mode-locked cavity. The trickiness of this particular instance of mode-locking is in the generation of two uncoupled pulses. The work presented in this dissertation has been conducted exclusively in free space cavities, so this subsection will be limited to this type. Also, it is important to note that a few groups have been able to create dual pulse, free space cavities by lasing simultaneously in orthogonal polarizations. This was not a possibility in this work since our gain mediums were all Brewster angle polished Titanium Sapphire (Ti:Sapph) crystals, which reject the vertical polarizations. While having the same polarization can lead to problems of injection locking due to scattering, it does prevent any incidental measurement of birefringence within the cavity.

With these restrictions, it is possible to choose an appropriate mode-locking mechanism. In early work, bi-directional Kerr Lens mode-locking was investigated. This technique was found to have a preferential direction, even to the point that it would switch back and forth between two directions, but never lase simultaneously in both. This resulted in decidedly single pulse operation [29][24]. The next most common way to mode-lock a laser is via a saturable absorber (SA). In this dual pulse operation, the pulses, in order not to lock into each other, need to travel in opposite directions throughout the cavity, known as counter propagating. This means that the SA will define a crossing point of these two pulses. It also means that the mode-locking is determined by both pulses interacting with the SA simultaneously. This is known as colliding pulse mode-locking. Since both pulses reach the SA surface at the same time, there is a great danger of injection locking at the SA [27]. Injection locking occurs when scattering from one beam is added coherently to another causing the two separate beams to lock to the same frequency. This is fatal in IPI systems as it destroys the phase difference between the two pulses. In order to avoid the catastrophic locking of the pulses, the SA must prevent coherent scattering. This can be achieved by utilizing a free-flowing dye-jet which scatters light incoherently out of the cavity. The free flowing nature of the jet randomizes the phase of the scattered light so that even the small portion that could interact with the pulses remaining in the cavity cannot do so coherently. For this reason, like the majority of my predecessors, I chose to use a free flowing dye-jet as my SA using the dye HITCI from Exiton© in a solution of ethylene glycol. This solution had its peak absorption around 740nm.

With these two elements in place, there is only one specification left that separates this setup from a unidirectional laser. It is vital that the pulses are created with equal, or as close to equal as possible, intensities. In the case where this is not achieved, each round trip, the stronger pulse will receive more and more gain while the weaker slowly dies. This Darwinian effect leads to unidirectional operation which is useless for IPI.

To avoid this phenomenon, the gain and the SA must be placed at an anti-node and a node of the cavity respectively. That is to say, while the pulses cross in the SA by definition, the gain must be placed at a location where the pulses are furthest apart in the cavity. This is known as an anti-crossing point and, in the case of a ring laser, is located a quarter cavity length away from the SA, or a crossing point. In the linear cavity, this is at a distance of one half the cavity length, or a quarter of the optical path length of the round trip, keeping in mind that in one round trip of a linear cavity, a single pulse traverses the cavity twice. With this last cavity adjustment, a cavity can become an IPI sensor of the type that was used for the work of this dissertation. It should be noted that an OPO cavity or a fiber based cavity are both capable of performing IPI measurements without a SA; however, for this work, the relative ease of simple adjustments to a free space cavity and avoiding tricky alignments where pulse crossing are vary sensitive to cavity lengths were considered less than ideal.

3.2 Application to Ring Laser Gyros

As stated previously, throughout the work that is presented in this dissertation, the main application of the IPI technique has been focused on the construction of a pulsed laser gyroscope. This section will serve to discuss the basic theory behind all optical gyroscopes, known as the Sagnac Effect, and explain how IPI is used to measure rotation rates, and why it is very well suited for this application. The sensitivity enhancement, which is the main objective of this chapter, will be discussed later in Sect. 3.3.

3.2.1 Sagnac Interferometry

Georges Sagnac was attempting to prove the existence of the aether in 1913 when he invented a sensor, now known as the Sagnac Interferometer. This device operates by

sending light around a closed ring in counter propagating directions and looking at the interference between the two beams. The equation for such operation is;

$$\Delta\phi \approx \frac{8\pi}{\lambda c}\mathbf{\Omega}\cdot\mathbf{A}, \tag{3.2}$$

where $\Delta\phi$ is the induced phase shift, λ is the wavelength of the light, $\mathbf{\Omega}$ is the rotational velocity, and $\mathbf{A}$ is the directional area [42][43]. While Sagnac never proved the existence of the aether, though he thought he did, he did invent the optical gyroscope, which measures the speed of rotation of a given cavity. For the rest of this chapter, I will use a version of Sagnac's invention to explore how the sensitivity of IPI can be manipulated.

3.2.2 Ring Laser Gyroscopes and IPI

Since the invention of the Sagnac interferometer, the optical and, more specifically laser community has capitalized on its use as a gyroscope. The theory is fairly easy to understand, and the basic example is simple to construct. By using the ideas of Subsection 3.2.1, the design of Subsection 3.1.3, and Eq. 3.2, this subsection will discus the construction and details of the first Ring Laser Gyroscope (RLG) used in this project.

This first cavity, whose schematic is shown in Fig. 3.2, was designed and constructed as a learning tool for me to fully understand the core concepts of the IPI technique. This basic cavity had a repetition rate close to 100MHz, and had no dispersion compensating prisms. The goal was basic; observe an IPI signal, or beat-note. This cavity was a true RLG in every sense, and yet, it could not rotate as it was built on a stationary rectangular optical table.

In reality, none of the cavities used in this project were capable of actually rotating. For this reason, a piece of 200μm Lithium Niobate was inserted into the cavity at Brewster's Angle. It was placed at an anti-crossing point and fed a square wave signal

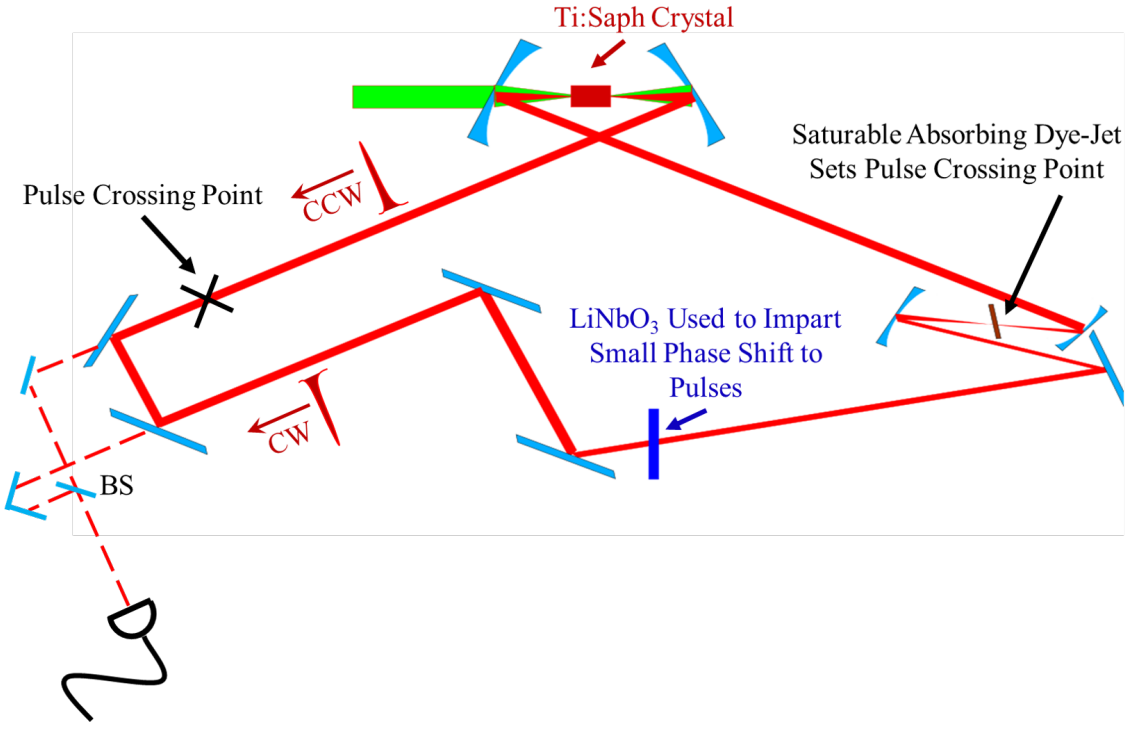

Figure 3.2: This schematic shows the first ring cavity I designed for IPI measurements. The solid red beams are the generated NIR light that oscillated around this cavity. The dashed lines are the delay line used to measure the interference of counter propagating directions. The green lines represent the pump laser that was focused onto the Ti:Sapph crystal. This cavity had a round trip time of approximately 10ns and achieved mode-locked operation via a free flowing dye-jet saturable absorber. The counter propagating pulses are depicted with an arrow showing their direction of propagation around the cavity as well as a label; cw for clockwise and ccw for counter clockwise.

that was triggered by the circulating pulses, whose amplitude could be controlled. The signal and the pulses are shown in Fig. 3.3. As shown by the equal pulse amplitudes, this setup has the gain and the SA very nearly a quarter cavity apart, as previously discussed, leading to a stable dual-pulse operation. This allowed us to simulate a rotating cavity as we could impart a differential phase shift to counter propagating pulses.

In this initial cavity, the beat-note was taken by interfering the leakage of two 45^o mirrors, as shown by the dashed red lines in Fig. 3.2. The advantage of this leakage is that it is very clear which direction is which, a technical point that was complicated

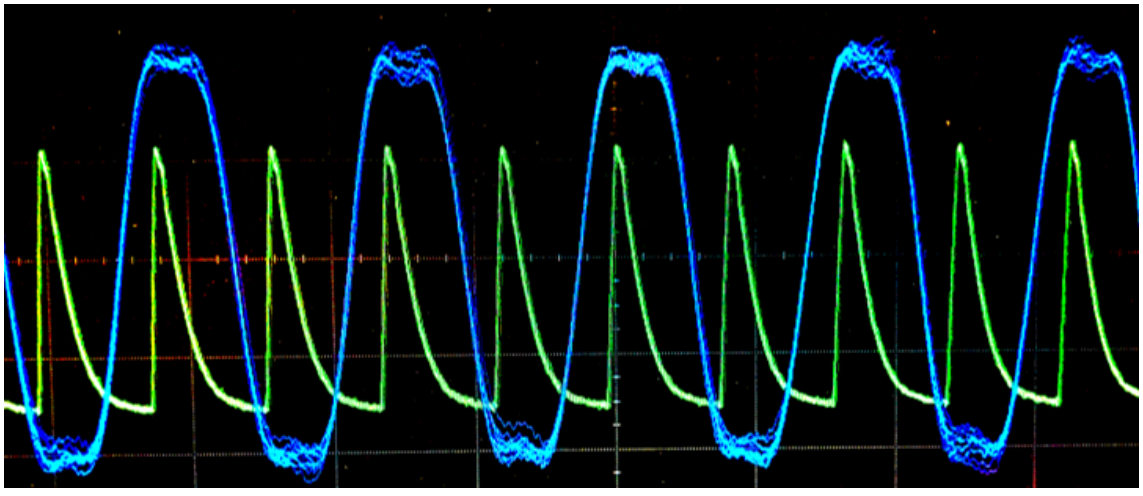

Figure 3.3: A photograph taken of the screen of an oscilloscope displaying the square wave signal sent to the Lithium Niobate, in blue, and both pulse directions sent to the same channel of the oscilloscope in green. The pulses are taken using a Thorlabs© model Det10A silicon detector viewing reflections of the Lithium Niobate. The Det10A possesses fairly slow sampling rate, thus the pulses appear quite large. Each consecutive pulse shown is traveling in the opposite direction from its predecessor. The equal spacing of the pulses, approximately 5ns, demonstrates that the Lithium Niobate is at the anti-crossing point, and it is clear from this photo that each direction is receiving a different voltage.

in some of the later designs. Since this leakage is not extracted at exactly the crossing point, it is necessary to build a precise delay line which can overlap the pulses in time at the detector. This is unnecessary in the CW case, where the laser emission is continuous, but crucial to the pulsed case, especially as pulses get shorter, leaving less room for error in the overlap.

The final point of interest in showing this cavity is the location of the second crossing point. In these cavities, the crossing point locations are fixed by the mere fact that the location of the dye-jet is stationary. This means that the opposite crossing point is always half a cavity away, since both pulses travel at the same speed. When designing these cavities, it is important to keep in mind where the second crossing point will be. As was discussed with the choosing of the mode-locking mechanism, if the pulses cross at a surface, it is possible to scatter light from one direction to the other, resulting in injection locking. For short pulses, this is easy to avoid; however,

as the pulses increase in length, the danger of injection locking increases. If any section of the pulses overlap, this occurs, so it is extremely important to design these cavities with the pulse length in mind.

3.3 Sensitivity Manipulations Via Resonant Dispersion

In Section 3.1 and Section 3.2, the IPI technique was introduced and explained, as was its application to RLG's and how to design such sensors. Up to this point, many of these topics were a background for the work that has lead up to the main work presented here. In this section, for the first time, the enhancement of the IPI sensitivity will be discussed, theoretically calculated and experimentally proved. I will also disprove a previous theory of the impact of the group velocity on gyroscopic sensitivity experimentally. The work presented in this section has been the subject of multiple grants, an afore mentioned patent [41] and a paper [37].

3.3.1 IPI Enhancement Theory

IPI theory amounts to a relatively simple equation, Eq. 3.1. A downside to such simplicity is that there are very few variables with which to attempt to examine the fundamental functionality. Much like in the case of the Sagnac Equation, Eq. 3.2, at first glance, it seems only the wavelength, cavity area, and perimeter can play an active role. Interestingly, the idea of shortening the wavelength, or moving to higher frequencies, has spawned some very interesting research into atomic and particle based gyroscopes[44][45], but this is outside the scope of this research.

In the case of this research, we specifically took interest in the variable τ_{RT}. The

Taylor expansion, to first order, of this value is;

$$\tau_{RT} = \tau_{RT,0} + \left.\frac{d\psi}{d\Omega}\right|_{\omega_0}, \tag{3.3}$$

where the initial round trip time is denoted as $\tau_{RT,0}$. The first order term, $\left.\frac{d\psi}{d\Omega}\right|_{\omega_0}$, is exactly the definition of linear dispersion. While this seems relatively uninteresting, this revelation gains huge significance when it is reinserted into Eq. 3.1. This is results in;

$$\Delta\omega = \frac{\frac{\Delta\phi}{\tau_{RT,0}}}{1 + \frac{1}{\tau_{RT,0}}\left.\frac{d\psi}{d\Omega}\right|_{\omega_0}} = \frac{\Delta\omega_0}{1 + \frac{1}{\tau_{RT,0}}\left.\frac{d\psi}{d\Omega}\right|_{\omega_0}}, \tag{3.4}$$

where $\Delta\omega_0$ is the beat-note before enhancement. This implies that for the presence of a resonant negative linear dispersion, *the beat-note signal of an IPI sensor can be, ideally, significantly amplified*. This amplification is limited by the width and slope of the dispersion.

This statement, though it sounds grandiose, does contain within it a few limiting factors. First and foremost, no one wants a beat-note signal at infinity Hz, that would be useless and impossible to measure. Another important point is that the dispersion must be resonant. This is actually amazingly crucial. The dispersion inserted into the IPI cavity must affect every tooth of the frequency comb in exactly the same way, but it must also affect the counter propagating combs in the exact opposite manner from each other. This type of resonant dispersion will be shown to be possible by utilizing the results of chapter 2, and will be detailed in Subsection 3.3.2. The final, and most important aspect of this statement, if signal enhancement is truly desired, is that the dispersion must be negative. This is perhaps the most challenging piece to accomplish, but without it, there will be no enhancement.

An important limitation of IPI enhancement in reference to laser gyroscopes is also apparent from examining Eq. 3.4 and comparing it to Eq. 3.2. The enhancement term in Eq. 3.4 is inversely proportional to the round trip time of the cavity, while

Eq. 3.2 is proportional to the cavity area. These two dependencies counteract each other which means that, while theoretically, you can counter the dependency on area by increasing the amount of negative dispersion, from a practical standpoint, this is only possible to a limited extent. Therefore, IPI systems in general can use this enhancement to scale to chip scale applications; however, this important capability is not true for the case of IPI gyroscopes.

In Fig. 3.4, a cartoon of how this enhancement works in the frequency domain is presented. In the top panel, both combs are initially shown as the red comb teeth,

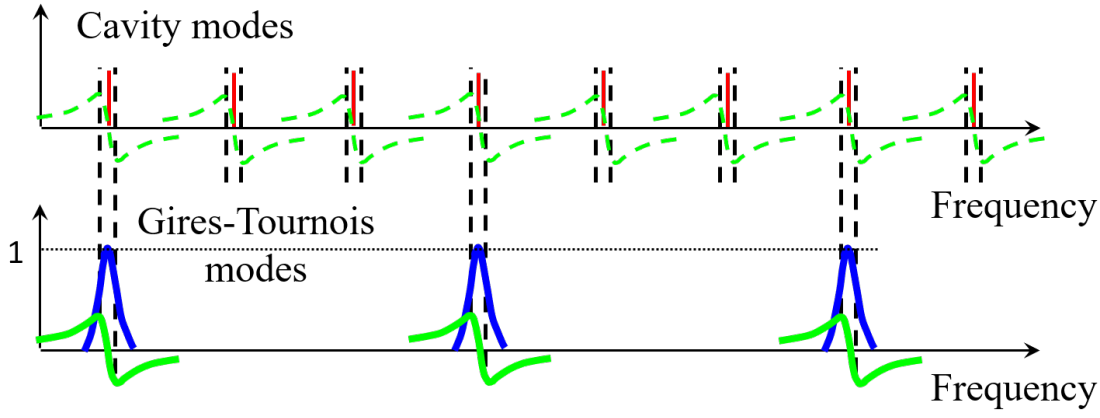

Figure 3.4: This cartoon illustrates how IPI can be enhanced through dispersion. The top panel shows the initial red comb lines before the directions observe any phase shift, for an RLG, this means the cavity is at rest. The black dashed lines show the IPI signal as the phase shift is added, or as the cavity begins to spin. Both green lines display the dispersion imparted to the combs on top of their phase shift. The ones in the top panel are dashed just to show that the dispersion of the two directions is, in fact, different. In the lower panel, the dispersion and its source, in blue, are shown together to illustrate that the dispersion does not have to occur at every comb tooth in order to affect every tooth.

identical to each other. The black dashed lines indicate the typical IPI sensors where the differential phase shift to be measured moves the twin combs with respect to one another. In the bottom panel, the blue lines show the resonance of the inserted linear dispersion and the green lines indicate that dispersion. The anomalous portion of the dispersion needs to be wide enough to cover both split teeth, but narrow enough that is does not overlap with the adjacent set of comb teeth. These resonances need

to occur at some, but as will be shown not all, of the comb teeth. The dashed green lines are meant to indicate that while only certain modes come in contact with the resonances themselves, all the teeth are effected in each comb. It is also worth noting that, due to the fact that dispersion is wavelength dependent, the anomalous dispersion will push the already separated teeth further apart, which is the case with negative dispersion. For positive dispersion, or normal dispersion, the teeth are actually brought closer together, which leads to a reduction in IPI sensitivity [37].

3.3.2 Enhancement through Resonant Dispersion

In Subsection 3.3.1, it was theoretically shown that a remarkable enhancement was possible in IPI sensors by adding resonant linear dispersion. Here I definitively prove the validity of this theory via a proof of principle experiment completed within the cavity shown in Fig. 3.2.

For this experiment, first an IPI voltage curve was taken by incrementally increasing the voltage difference sent to the Lithium Niobate and recording the resultant beat-note frequency. The voltage difference was varied from low to high values by adjusting the amplitude of the square wave via a fast, high frequency amplifier. Since this was only a proof of principle and negative dispersion can be quite tricky to insert into a cavity, an FPE was inserted into the cavity. As was discussed in chapter 2, in order for a cavity to mode-lock with a nested FPE, the laser cavity must be resonant with both the larger cavity and the FPE. The FPE that was used was found, through calculation, to have a linear dispersion of $\frac{1}{\tau_{RT,0}}\frac{d\psi}{d\Omega}\Big|_{\omega_0} = 1.9$ at the central wavelength, calculated via;

$$\frac{d\psi}{d\Omega} = \frac{1+r}{1-r}\frac{nd}{c}, \tag{3.5}$$

where r is the $\sqrt{R}$, and R is the reflectivity of each face of the FPE.

Fig. 3.5 shows the results of two voltages curves that were taken with, the blue curve, and without, the red curve, a nested FPE. By comparing the slopes of these

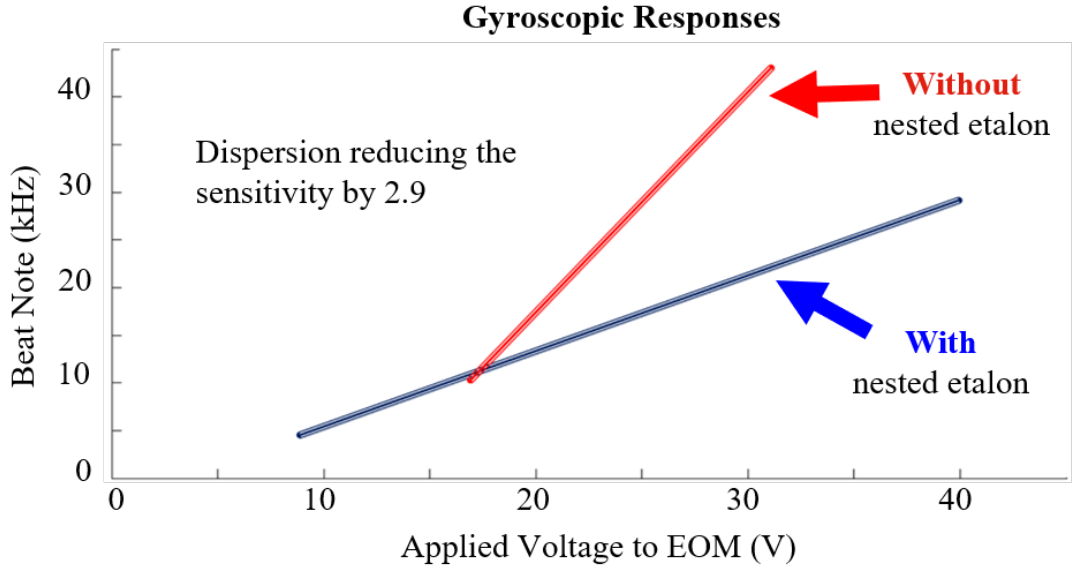

Figure 3.5: This figure shows the first published voltage curve demonstrating the ability to alter the sensitivity of IPI. In this experiment, an FPE is nested into the RLG and the reduction in sensitivity is found to identically match the dispersion induced by the FPE.

two curves, we found that the sensitivity had been reduced by a factor of 2.9, which is exactly what we expected from Eq. 3.4. Multiple FPE angles were tested, all yielding the same result.

This was the first proof of enhancement of an IPI sensor to be published [37]. With this result, we quickly moved to achieve a resonant negative dispersion for a final proof of the validity of this project and to achieve an ultimate sensitivity surpassing that which has previously been achieved from similar setups.

3.3.3 Disproving Fast/Slow Light Enhancement

Many theories exist surrounding the most effective ways to increase the sensitivity of laser gyroscopes. One that has surfaced a lot is the idea of changing the speed of light within a cavity. This is typically known as Fast or Slow Light, depending on whether the speed is being increased or decreased. In the interest of completeness, I have decided to address this topic here.

First, it should be noted that many of the publications on this topic in the past have been theoretical [46][47]. Recent publications have shown success using negative dispersion techniques; however, these results were all accomplished using CW lasers [48][49]. This latter point is important because the idea of light speed enhancement relies on the group velocity and group dispersion of a given light source. As was already stated in Section 2.3.1 of chapter 2, group velocity requires there to be more than a single frequency. This means that the mathematical definition of $v_g = \frac{dk}{d\omega}$ requires there to be more than a single ω. Therefore, these recent results of sensitivity enhancement are more a proof that the phase dispersion, not the group dispersion, is responsible for the observed enhancement. All of this may seem trivial, but it is a common error found in numerous gyroscope papers. The end result is that speed of light enhancement requires the existence of pulses; therefore, the lack of slow light enhancement is CW laser gyroscopes should not be surprising at all, and looking for such enhancement in these systems is a waste of time.

As it happens, my IPI gyroscope is a pulsed laser system, and, when a FPE is nested inside, is quite capable of comparing the beat note signal of various cavity repetition rates. As shown in chapter 2 in Fig.2.5, adjusting the angle of the FPE can have a large effect on the cavity repetition rate, and thus the group velocity of the oscillating pulses and envelop velocity of the bunches. In Fig.3.6, the results of such an experiment are shown. The repetition rate of the cavity clearly changes with the angle of the FPE, as shown by the red curve, while the beat note slope, the blue

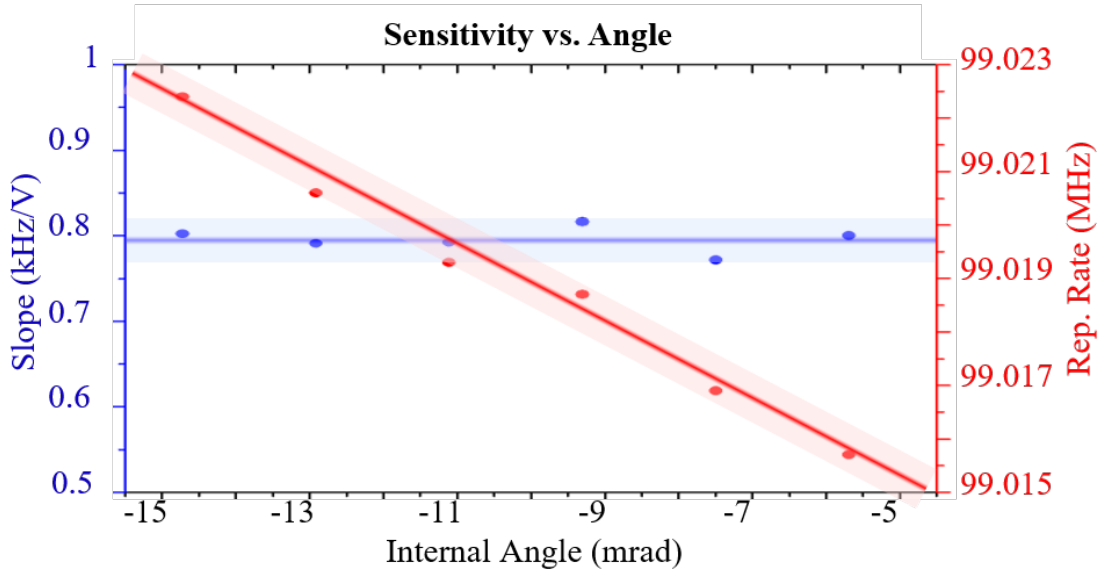

Figure 3.6: The data presented in this plot clearly demonstrates that the concept of fast/slow light has no effect on the sensitivity of IPI. For this experiment multiple voltage curves were taken at varying angles of the nested FPE, effectively changing the repetition rate of the RLG, shown in red. As shown by the blue curve, the slope, and therefore the IPI sensitivity, is unchanged by this change in repetition rate.

curve remains flat. This indicates that the sensitivity of the system remains unchanged.

While this data says nothing about a CW system, it does prove conclusively that there is no measurable speed of light enhancement for IPI laser gyroscopes. This was the first demonstration, that I know of, of this lack of enhancement [37].

3.4 Creating Resonant Negative Dispersion

A number of methods exist that can create a negative dispersion at 800nm. First, most absorption results in negative dispersion. Absorption also means adding significant loss to the laser. Another, more accessible method would be to use the FPE in reflection instead of transmission. This can be understood by revisiting Eq. 3.5 and solving for the case where the front and back faces have different reflectivities. This

solution and was found as part of a larger analysis done by Mr. Luke Horstman in an effort to theoretically optimize IPI enhancement. The solution goes like;

$$\frac{d\phi}{d\Omega} = \frac{2nd}{c} \frac{\alpha\beta - \alpha\gamma\cos\delta}{(\alpha\sin\delta)^2 + (\beta\cos\delta - \gamma)^2}, \tag{3.6}$$

where α is $r'(1-r^2)$, β is $r'(1+r^2)$, γ is $r(1-r'^2)$, and δ is the phase term and is approximated as $-2kd$. In these definitions, r and r' are the front and back electric field reflectivites respectively.

The device described above is known as a Gires Tournois Interferometer (GTI), and requires light to be normally incident. Such a requirement means that we must add a location to our laser where light is normally incident on a mirror. For this reason, we constructed the linear laser shown in Fig. 3.7.

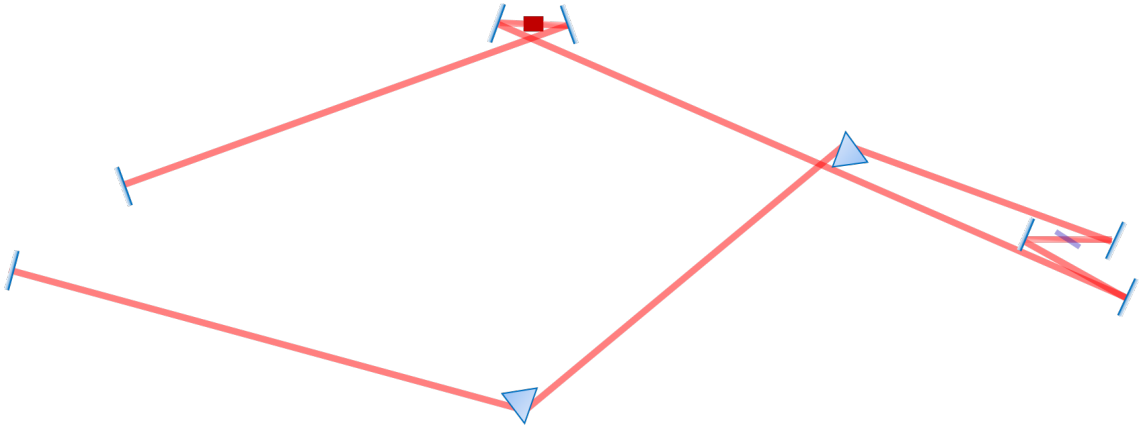

Figure 3.7: This is a schematic of the original linear laser used to test the Gires Tounois Interferometer (GTI). The Ti:Sapph gain crystal, prisms, and dye-jet are all the same, the ring is no longer closed. This linear cavity is necessary to have a place in the cavity where the GTI can be an end mirror.

This cavity was selected since it seemed like it would be easier to prove the enhancement abilities of a GTI in a linear cavity. As will be seen in Subsection 3.4.1, this cavity yielded somewhat strange results when we attempted to replicate the original reduction results. This cavity had the same properties of the ring shown in Fig. 3.2, except that the ends were not joined. While this cavity has yielded some

advancements in our understanding, it is still a curiosity that it could not replicate the original results and has pushed us to the ring design that will be shown in Fig. 3.9.

3.4.1 Observation of True Enhancement

Upon the completion of the cavity shown in Fig. 3.7, a series of IPI curves were taken with various resonantly dispersive elements, the results of which are shown in Fig. 3.8. The data presented in Fig. 3.8 was taken in the order of the run number shown along

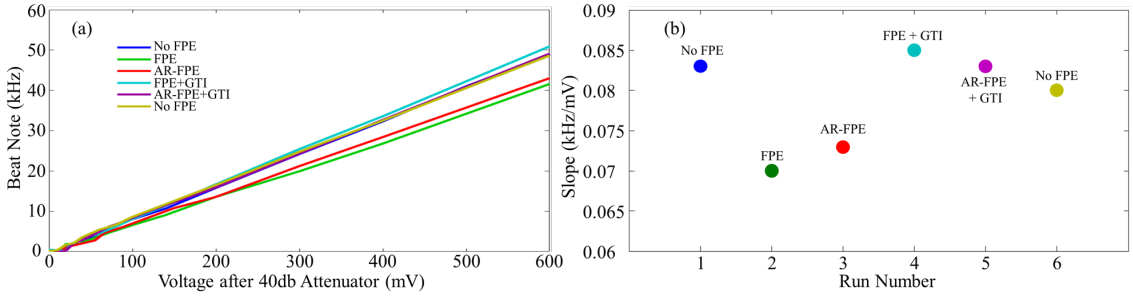

Figure 3.8: This is the first evidence of enhancement of an IPI sensitivity due to resonant negative dispersion. Part (a) shows the lines that are used to calculate the slope values in part (b). For each run, a different combination of Gires-Tournois Interferometer (GTI) and FPE were used. Runs 1 and 6 were done as controls without any added dispersion, and were done before and after all data was taken, respectively to give an idea of where to control cavity sensitivity was. As expected, the regular FPE and the Anti-Reflective (AR) coated version (AR coating at 800nm), both reduced the sensitivity when placed in the cavity alone. The reduction from the AR-FPE was less than that of the uncoated version. The uncoated FPE with the GTI, when the FPE was tuned close to the resonance of the GTI, was shown to clearly have a sensitivity above both control runs. the AR-FPE with the GTI was shown to have reduced enhancement under the same conditions; however, this combination definitely did not reduce the sensitivity.

the x-axis. The y-axis is the slope of the IPI data where the beat-note is measured as the voltage difference on the Lithium Niobate is increased. The first and final runs (runs 1 and 6), the blue and yellow points respectively, are taken for the same cavity condition of no resident dispersion at the beginning and end of the experiment to show see the variance in the control condition.

Runs 2 and 3 were done to reaffirm the conclusions of Fig. 3.5. Run 2, the green is for the same FPE nested in the ring as before, to reaffirm that the reduction is similar. While the reduction was indeed present, it was nearly half of the value that we had in a ring IPI system. This is due to the fact that since we are now in a linear cavity, the τ_{RT} is nearly doubled. In run 3, the red point I tested of the amount of reduction present when an FPE is used with an anti-reflective (AR) coating. As expected, this reduction in dispersion reduces the amount of reduction due to the nesting of the FPE. In run 4, the turquoise point, the uncoated FPE is inserted with a GTI as an end mirror. The FPE is then tilted to a point where it seems close to resonant with the GTI. This is done by monitoring the beat-note frequency as the FPE is tilted. It is shown in the plot that this point is at a visibly larger y-value than any other point, including the two control points. Therefore, this is the *first* observation of enhancement of an IPI system. Run 5, the purple point is done using the same method as run 4 only with the AR-coated FPE. Just as the amount of reduction was reduced in the case without the GTI, the amount of enhancement here is reduced, putting the slope almost at the same level as the first control point.

The data presented here is not only the first experimentally observed enhancement of IPI, but it is also the preliminary ground work for a future free space IPI experiment using a dye-jet and a ring laser with a tail. This, and other future IPI enhancement experiments are outlined in Subsection 3.4.2.

3.4.2 Future Methods

In the immediate future and keeping with a free-space dye-jet cavity, there are a few more experiments that we would like to try that have proven pretty difficult thus far. These experiments, if successful, will be the last to take place in this cavity. Future ideas for IPI will be discussed in the conclusion of this chapter.

Ring Laser with a Tail

The first thing to try is to go back to a ring setup and see if this data holds. In order to have a GTI in a RLG, a tail must be added to have a point of normal incidence. A cavity of this description is shown in Fig. 3.9.

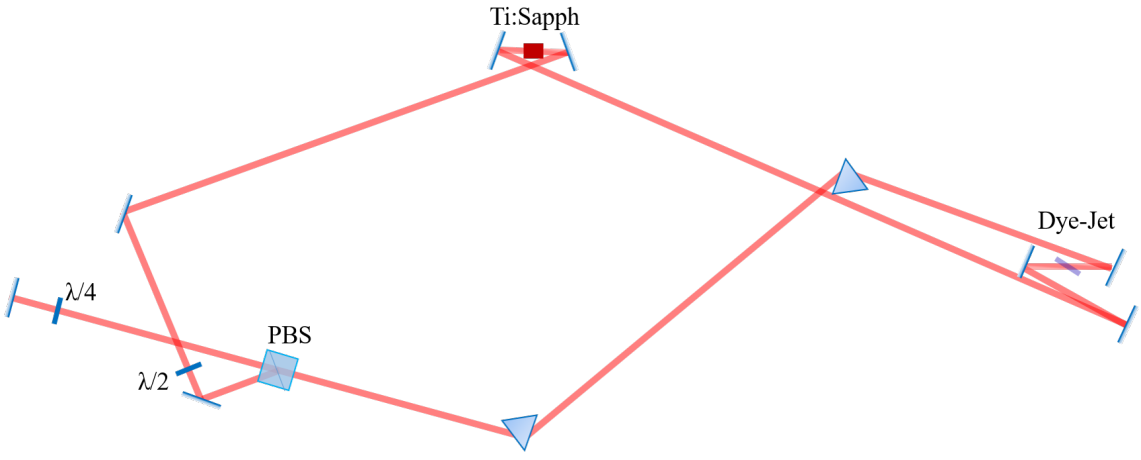

Figure 3.9: This is a schematic of the ring laser with a tail. The Ti:Sapph gain crystal, prisms, and dye-jet are all the same as in Fig. 3.7, but now a Polarizing Beam Splitter (PBS), a half wave-place ($\lambda/2$), and a quarter wave-place ($\lambda/4$) have been added to make a tail. This tail is necessary to create a place in the cavity to insert the Gires Tounois Interferometer (GTI) as an end mirror.

The cavity drawn in Fig. 3.9 propagates light in the following way. Emission from the Ti:Sapph is horizontally polarized due to the fact that it is cut at Brewster's angle. If we travel in the clockwise direction, from the gain to the dye-jet to the Polarizing Beam Splitter(PBS), the laser is incident on the PBS with horizontal polarization. Then, a double pass through the $\lambda/4$ rotates the light to the vertical polarization, which is reflected by the PBS. Finally, the $\lambda/2$ is necessary to rotate the light back to the horizontal polarization in order for it then to pass through the Ti:Sapph with minimal loss.

The light traveling in the opposite direction, since this is still a bi-directional laser, is rotated similarly. It is first incident on the $\lambda/2$ rotating it into the vertical

polarization before it reaches the PBS. Vertical polarization is reflected by the PBS, injecting this light into the tail so that it undergoes a double pass through the $\lambda/4$, rotating it into the horizontal direction, in which state it is transmitted through the PBS and allowed to travel through the rest of the cavity.

Having a tail in a ring cavity leads to some interesting tuning capabilities. The end mirror of the cavity can be either a normal wedged mirror, or a GTI, depending on the purpose the cavity is being used for. It is also relatively simple to adjust the length of the tail. Finally, the presence of the rotatable $\lambda/4$ allows the cavity to go from a ring design to a linear design relatively easily. This is because, without the $\lambda/4$, the light exits the tail with the same polarization as it entered with, and, therefore, travels back in the same direction in came from.

Stabilizing an RLG with GTI

One reason why more enhancement was not observed in the preliminary measurements of Fig. 3.8 is that the cavity was not optimized for the GTI. Unlike in the case of a nested FPE, the GTI angle cannot simply be tuned, and, since the front face has a high reflectivity, the laser can mode-lock without becoming resonant with it. In the linear cavity, tuning the FPE angle gave us a result of near resonance which produced a small enhancement; however, the presence of the nested FPE also means that we were starting from an already reduced sensitivity, not to mention that the FPE and GTI possessed different thicknesses. In order to see the large enhancement that the theory predicts above the empty cavity, we are going to need to do better.

To that end, we have begun construction of the ring laser with a tail shown in Fig. 3.9, but this is not enough. The repetition rate of the larger laser cavity must be resonant with that of the GTI. For this to work, a stabilization loop must be attached to a piezo mount to hold the GTI. This feedback loop seeks to maximize the leakage

of the GTI, since its transmission is maximum at resonance.

This last point may seem problematic, since a large transmission for an end mirror in a laser would effectively disrupt all lasing; however, it is our belief that as the GTI becomes more transmissive, there will be a point where the laser power begins to decrease. In this case, it should be possible to be resonant enough to observe some enhancement by locking to the highest leakage, even though this would not be the theoretical maximum.

Negative Dispersion Via Two Photon Processes

There are other options for creating negative dispersion. Both of these alternative are based on the fact that absorption peaks tend to have a negative dispersion associated with them.

The first of these alternatives is to insert a second harmonic crystal into the cavity. The resultant two photon absorption has an associated negative dispersion. While a perfectly phase matching would amount to a major loss to the cavity, this alternative does not require high efficiency conversion, just enough to create a negative dispersion curve. Since high conversion efficiency is not a necessity, it is possible that no extra focusing will be required in this method. Therefore, the lack of a lot of extra components within the cavity makes this proposal attractive at the outset. On the other hand, using the internal laser energy to generate second harmonic light is a loss to the laser, and so the laser will only stay at this wavelength if it is stabilized in the manner described above. Still, the amount of total loss in this scenario should be less than that for the GTI and the length of the SHG crystal does not need to be resonant with the larger laser cavity. The problem with this proposal is that the phase matching bandwidth should be smaller than the mode spacing, which implies a second harmonic longer than τ_{RT}.

The second alternative is similar to this first idea. It is possible to do two photon absorption within an atomic vapor cell. Our group, as demonstrated already, has lots of experience dealing with ^{87}Rb, and this is an ideal candidate for a Ti:Sapph ring laser cavity. This adds greater functionality to the IPI setup. While using a vapor cell requires heating and Helmholtz coils to control the atomic states, it does also mean that we can use the vapor cell as a magnetic sensor in the IPI cavity, similar to the previous work done with a Terbium Gallium Garnet(TGG) crystal [35][36].

Both of these suggestions should yield significant enhancement in IPI. While each has drawbacks, what they bring in terms of capabilities to this technique, I believe, outweigh their short comings.

3.5 Conclusion

Intracavity Phase Interferometry is a powerfully diverse and sensitive phase measuring technique. The main drawback has been that it has been confined to large optical cavities on bulky optics tables. With these new enhancements, the equations that have tied sensitivity to cavity length no longer condemn these sensors to basement laboratories. As more efficient enhancement methods are discovered and implemented, smaller and smaller cavities will be possible which weigh less and are portable.

Already, talks of collaborations in integrated circuit cavities utilizing resonant negative linear dispersion are underway, while others within this research group are working to implement durable fiber cavities. There is also an effort to move back to OPO cavities rather than laser dye-jets to avoid these messy elements that can be very temperamental and cause many practical issues in the lab. These new cavities will push this technique out of the lab and into the field. This latest push for more portable, robust, and small systems would not be possible without the discovery of

linear enhancement methods.

Such a diversity of cavities is actually a requirement to reach all the possible areas where IPI can be an useful tool. We have shown here that a gyroscope is a definite possibility as an application of this technique. Being able to create very small gyroscopes would be an amazing advancement for the transportation and navigation industries. IPI has also been previously tried and tested as a magnetic sensing technique. This type of application may be quite difficult to make chip-scale; however, moving to solid-state and fiber cavities could lead to much less bulky systems than those currently in use, and, with enhancement, could prove to be much more sensitive. These are just two examples of the great diversity of applications where IPI can prove useful. Anything that can cause a differential phase shift within a cavity can be measured using IPI, and these possibilities are, as of yet, uncountable.

More work is needed to discover where the limit of these enhancements will be and to find the best ways to implement them. These solutions will likely be different for the large variety of cavities mentioned. As these enhancements have come to light and systematically been proven, the interest in IPI has slowly grown, and it is my hope that with this steadily increasing support, this technology will become more accessible in a wide assortment of areas of study.

Chapter 4

Conclusion

> Long is the way and hard, that out of Hell leads up to light.
>
> – John Milton, Paradise Lost

This dissertation has demonstrated conclusively the strength, stability and flexibility of nested cavities and tailored frequency combs. They have been characterized, their inherent stability has been quantized, their tuning has been more deeply explored, and their usefulness in metrology have been investigated and proved. In this concluding chapter, these advancements and discoveries are outlined and some future possible applications and investigations are described.

4.1 Summary

Throughout this dissertation, there have been two main focuses. The first was the characterization and quantification of certain aspects of nested cavities and their resultant unique comb structure. The second focus is married to this idea, but conceivably separate in practice. This, of course, is the idea of Intracavity Phase Interferometry (IPI) enhancement through resonant linear dispersion. While this dissertation

centers around achieving this through nested Fabry-Perot etalons (FPEs), it is conceivable that others methods exist or could be discovered to achieve this enhancement.

Nested Cavity Results

In relation to nested cavity characterization specifically, there are four main novel discoveries that have been demonstrated. The first is the general greater characterization of tailored frequency combs in the rf and optical domains. The optical comb had never been directly observed before the work presented here and the cavity coupling, as investigated via the rf domain, has increased our understanding of the connection between two nested cavities.

Secondly, I have demonstrated interesting characteristics in the time domain. Specifically, the dependence of the number of pulses within a bunch to the internal angle of the nested FPE, as was shown in Fig. 2.5. This study also demonstrates how the repetition rate of the cavity changes depending on whether it is in pulse bunch operation, single pulse operation, or, interestingly, two pulse operation.

Thirdly, this dissertation also contained a number of simulations that predicted the shape of the pulse bunch as well as the location and value of different frequency modes. The latter was demonstrated by first accurately predicting the FPE angle values of ^{87}Rb fluorescence peaks and then by predicting the shift of these peaks due to temperature changes. These two demonstrations show not only the predictability of these combs, but also their usefulness in index measurements and atomic state tuning.

Finally, the passive inherent stability of modular comb structures was demonstrated and quantized. This is the first demonstration of this kind, indicating incredible stability of internal comb structures, especially with regards to a sideband structure's

relation to its central nested frequency, or the relationship between the MHz structure to the GHz structure. While this method does not stabilize the CEO of the modular comb, it does indicate that these structures, comprised of two separate frequency elements, have an internal stability the begins to reach the values of actively stabilized cavities and that the repetition rate of a nested cavity is more stable than a standard cavity.

Although this dissertation does not prove it outright, the ability to determine the change of refractive phase index of the nested cavity independently from its length is shown to be possible. The underlying assumptions of the simplified super ratio are proven through these stabilization results. This coupled with the Rb peak fluorescence results show the presence of all necessary elements for this method.

IPI Enhancement Results

As far as advancements to the metrology technique of IPI are concerned, this dissertation has demonstrated three major points. The first of these was the predicted and observation of IPI sensitivity reduction due to a resonant dispersion. Before this work, the sensitivity of IPI had never been manipulated in such a fashion.

Related to this first observation was the demonstration of the lack of an effect on the sensitivity of $slow/fast$ light. There are a plethora of papers attempting to enhance the sensitivity of laser gyroscopes through manipulations of the speed of light that are backed up by a lot of federal government funding. Therefore, the result that the internal angle of a nested FPE, which controls the group velocity, has no effect on the sensitivity of the IPI sensor is a major result.

Finally, the most important observation of this dissertation is the proof of enhanced sensitivity due to resonant dispersion shown in Fig. 3.8. While this first observation

only shows the cancellation of sensitivity reduction with only mild improvement over the bare cavity sensitivity, it is the first such demonstration that such an enhancement due to negative resonant linear dispersion is possible for these IPI sensors and was the ultimate goal of the work that has been conducted for the last five years. This is the culmination of an effort to show an effect that was predicted, mathematically, years before and, after many different cavity designs and studies into the behavior of nest combs, finally lead to this positive result.

4.2 Future Projects

The results that have been detailed and presented throughout this dissertation have opened the doors to a wide variety of future projects, a few of which are already under investigation. All of the projects that I have chosen to include here are direct results of the work that is contained within this document. The purpose of including these proposals here is to both inform the reader of the importance of the research that has been done and the wide range of applications that it aims to influence.

Future Projects for Nested Cavities

While the main focus of this dissertation, from an application point of view, has been targeted at phase sensing projects for IPI, many of the results attained from these studies into the nested cavity configuration as well as the modular comb structure have sparked some interesting ideas for future projects. The projects that are listed here have already been discussed in various circles, though none of them have commenced at this time, to the best of my knowledge. It is my hope that all of them would be investigated as I believe they will yield interesting results and prove, on a wider scale, the importance and usefulness of tailored combs.

The first project is the construction of a stabilized tailored comb source using many of the ideas from the end of Ch. 2. In fact, this section even lays out some of the details of such a cavity as a motivation for some of its results. The basic premise would be to stabilize a comb structure without broadening the comb. Instead, the comb could be stabilized to the peak fluorescence of a ^{87}Rb which would feed back to a nested FPE. This could be accomplished through a variety of methods from tuning the angle with a piezo motor to quickly adjusting the FPE's refractive index. This latter idea would require an etalon whose index could be modified by applied voltage. Early in my initial index investigations, the idea of modifying an FPE's index by voltage was considered using a FPE of Lithium Niobate which was available in the lab. This was abandoned initially due to the difficulty in aligning the cavity. I believe that now that we have attained positive results from other cavity characterizations, that it may be time to revisit this idea.

Another possible project comes from the idea of perfectly harmonic cavities. Thus far, the work that has been presented used a parent and a nested cavity whose repetition rates were chosen somewhat arbitrarily with respect to each other. In the end of Ch. 2, there was a discussion of coupled cavities. In that discussion, it is shown that the repetition rates of two nested cavities can be made to approach an harmonic of each other. If this were to be achieved, then instead of pulse bunches, the laser would produce a pulse train at the repetition rate of the FPE. This means that a cavity could be made arbitrarily long to fit a given application and still be able to produce pulse trains at or above the current resolution of electronics. Such cavities have already been constructed in fiber, though not using the nested cavities that are investigated here [50][51][52]. In these other cavities, the ability to go to a pulse bunch operation is not a possibility, making this proposal novel. I have already performed a basic attempt to achieve this idea with a nested FPE. This initial attempt failed, primarily due to the fact that the front face of the FPE reflected the fluorescence back into the gain and fatally affected the mode-locking. To avoid this in the future, I would recommend using a GTI as an end mirror instead. This would preserve the

mode-locking and then the tuning of the cavity would be controlled by the end mirror position. These cavities could potentially be used as solid state stable GHz comb sources for lab applications requiring fast repetition rates and stable cavities.

Finally, the index metrology experiment outlined at the end of chapter 2 failed to actually find the change in phase index. Throughout this experiment, it was discovered that the various portions of the ratio equations were stable as predicted. It was also found that the fluorescence peaks move with respect to the internal angle of the FPE as predicted by a change in the phase index of the FPE. This leads us to the conclusion that this experiment is fundamentally possible with a correctly engineered cavity. Therefore, this dissertation proposes that an investigation into a more suitably engineered cavity be conducted.

Future Projects for IPI Enhancement

It is obvious from the sheer number of patents, papers, and dissertations on the subject that IPI can be applied to an immense number of applications. Rather than attempt to list these in this section, I will instead simply propose projects that could potentially improve on the enhancement techniques outlined in this dissertation and suggest cavities that might prove more helpful in exploring these other applications. All of the suggestions discussed here have either been discussed within our group or we have already begun investigating.

The first project is to build a new ring laser with a tail containing a GTI as an end mirror. This cavity, unlike the results demonstrated in the previous chapter, will be made resonant with the GTI via a stabilization feedback loop that maintains maximum transmission of the GTI. This choice of stabilization is due to the fact that the GTI transmission will be maximum at resonance. This project is currently underway, although the ring has proven quite difficult to align. The benefit of this

over the previous results is that it does not require a nested FPE, so instead of having to beat the positive dispersion of an FPE before starting enhancement, we can see enhancement immediately.

The next two projects are tied together in that they are based on the same principle, namely that absorption typically exhibits negative dispersion. The first of these is utilizing ^{87}Rb vapor as an absorber. By using a two photon transition, every comb tooth can be made optically resonant. That is, a central tooth sees a transition that is its second harmonic, and so two photons of this frequency are required to be absorbed. Since comb teeth are equally spaced, the two teeth on either side of this tooth can also sum together to be resonant with this transition. This continues with each pair of sequential teeth within the comb, thus ensuring that the entire comb is resonant with this negative dispersion.

One major caveat to this project is that this absorption is seen as a loss by the laser. This means that in order to stay resonant to the necessary transition, the same feedback loop required for the GTI is also required here. In this case it will maximize the generation of blue light emitted by the ^{87}Rb.

Finally, a project that is currently underway within our group is taking the fundamental enhancement techniques that have been discovered through these studies to more robust cavities. Currently, there are attempts underway to create IPI cavities in OPO systems, which removes the need to have a free flowing dye jet. This greatly increases the ease of alignment of the IPI sensor. Other attempts are targeted at creating fiber based IPI sensors which would allow for a portable IPI system and increases the number of applications that this technique can be applied too. These new cavities all have their own unique challenges and complications; however, the lack of a dye jet is a move towards IPI sensors capable of operating outside of the laboratory environment.

The work presented in this dissertation has lead to advancements in both the study of frequency combs and frequency comb metrology. The enhancements to IPI has helped spur on new projects within our group as well as encourage collaborations with other groups outside our university. These reported results have already yielded multiple publications, approved grant proposals, and a patent. With this recognition and the plans already in place to implement, the conclusions of this work are sure to aid and contribute to future studies in these fields.

Appendix A

Frequency Comb Stability

This appendix is included to provide a method for quantifying the stability of a frequency comb. The work in this dissertation utilized the calculation of the Allan Deviation to assess stability of frequency data. This method is presented here along with a motivation of its use in the projects of this dissertation, via a brief historical overview, and list of useful sources in order to clarify data presented in Ch. 2.

A.1 Allan Deviation Historical Overview

The Allan Deviation is a statistical method used to quantify the stability of a frequency generated by an oscillator over a specific period of time, τ. As τ is varied, the resultant plot of the Allan Deviation values has been used to identify the dominant noise sources for a specific time ranges. This is useful when attempting to stabilize a given frequency from an oscillator for a precise time period, for example, when designing a laser cavity that will be used to probe an atomic ensemble, the cavity only needs to be ultra stable for a short period.

Allan Deviations were first introduced by Dr. David W. Allan in 1966 as a method

for quantifying the stability of oscillators and characterizing their noise sources [53]. It appears, from the historical citations, that this method remained mostly internal to the Time and Frequency Division of the National Bureau of Standards, now known as the National Institute of Standards and Technology(NIST), for the following decade or so. Throughout this time, it was mainly used to quantify the stability of atomic clocks, as evidenced by a conference proceeding from 1974 [54]. In this document, Allan Deviations were used to compare 8 cesium clocks over a period of days resulting in Allan Deviation values on the order of 10^{-14}.

In the following decade, a description of this stability quantization method found its way into a progress report from the National Aeronautics and Space Administration(NASA), which reviewed various different methods of frequency stability measurements and noise characterization techniques in use by the organization [55]. At this point, it is safe to say that Allan Deviations had become a common language amongst the frequency stabilization community. This very handy calculation is now used broadly by the frequency comb and atomic clock communities in a multitude of publications; however, it often appears with little to no explanation or context. Even the equations used to calculate these values are often left out. An example can be found in a recent paper where an Allan Deviation of 10^{-18} over a period as low as 10^{-24} seconds is quickly reported in text and plots but without any mathematical context [17].

Due to its colloquial nature within this field of research, a full description of the Allan Deviation is left out of the main body of this dissertation; however, it has been included here both for completeness and as a reference for future students who wish to understand these results and why they are quantified in this manner.

A.2 Allan Deviation Calculations and Measurement Methods

The best resource I have found for learning about and calculating the Allan Deviation is an online document provided by NIST called "Properties of Oscillator Signals and Measurement Methods," by D.A. Howe, D.W. Allan, and J.A. Barnes [56]. The explanations are very clear and concise and it even provides examples to help walk you through the procedures. The calculations done throughout my dissertation research, and thus, what will be described here can be found in Section 4 of this document. I will not go into the relations to the standard deviation or the noise characterization in this appendix as these were not used in my research, though these may also be located in Section 4 of the cited document.

To calculate the Allan Deviation of a frequency, first the frequency must be recorded for a period of time that is much longer than the period of interest. During this, the frequency should be recorded in intervals *at least* as small as the period of interest. While the former is to ensure that there is enough data to average over as this is a statistical method, the latter can be very tricky and is typically limited by the equipment used to record the frequency. In this dissertation, two frequencies were examined, as well as their ratio. The first was the repetition rate of the laser. This was accomplished by periodically requesting this data from a frequency counter. The second was the repetition rate of the nested cavity. This was done by examining the rf frequency comb on a spectrum analyzer and watching the peak associated with this frequency. The fastest possible acquisition was on the order of 10^{-6} hours. These results are shown in Fig. 2.12. In both cases, the minimum Allan Deviation value was not achieved. Since this value is necessary to do the noise characterization, as this involves looking at the curve and slope around the minimum value, noise characterization was not conducted.

Depending on why the Allan Deviation is being calculated, different acquisition times may be necessary. For example, in the conference proceeding from 1974, cited above, τ is on the order of days as it was important to understand and quantify the long term stability of different atomic clocks [54]. However, in the publication from 2018 that was also included in the previous section, the interest was on determining the time scales at which the frequency was *most* stable and what noise sources dominated this region [17]. For this type of analysis, it was necessary to probe a much faster time scale. In the case of this dissertation, we were interested in seeing how different lasing operations compared to each other as well as the stability of various frequency components with respect to each other. For this purpose, it was not necessary to go to such short time scales, nor was it necessary to go as long as days, since our laser cavity was designed to operate on the minutes to hours time scale. For this reason, our data is presented with a τ on the order of hours.

Once the data is collected, it must be split into even chunks of time periods. This is calculated as;

$$< \nu >_i (\tau) = \frac{\nu_{i+1} - \nu_i}{\tau}, \tag{A.1}$$

where ν is a frequency value, i is a simple integer denoting the location in a data set of ν_i, and τ is the period of time. In order to calculate the Allan Deviation of a full data set accurately, the operation described in Eq. A.1 should be carried out across the entire set [56].

The new set, $< \nu > (\tau)$, can then be used to calculate a single Allan Deviation value for a single τ by plugging it into:

$$\sigma_{Allan}(\tau) = \sqrt{\frac{1}{2M-1} \sum_{i=1}^{M-1} (< \nu >_{i+1} (\tau) - < \nu >_i (\tau))^2}, \tag{A.2}$$

where M is the length of $< \nu > (\tau)$ [56]. Eq. A.2 is known as the Allan Deviation. In order to create a plot of Allan Deviation versus time, simply vary the value of τ

and repeat this procedure.

While it was not used in this dissertation, it should be noted the $\sigma_{Allan}(\tau)^2$ is known as the Allan Variance. This value is sometimes also used in publications, though not as frequently.

This is the procedure that was followed in order to calculate the plots that are found in Ch.2 of this dissertation. I have also written a MatLab© function that I can make available if requested.

References

[1] I. S. Ruddock and D. J. Bradley. Bandwidth-limited subpicosecond pulse generation in mode-locked cw dye lasers. *Appl. Phys. Lett.*, 29:296, 1976. 2

[2] J.-C. Diels, J. Menders, and H. Sallaba. Generation of coherent pulses of 60 optical cycles through synchronization of the relaxation oscillations of a mode-locked dye laser. In R. M. Hochstrasser, W. Kaiser, and C. V. Shank, editors, *Picosecond Phenomena II*, page 41, Berlin, 1980. Springer-Verlag. 2

[3] W. Dietel, J. J. Fontaine, and J.-C. Diels. Intracavity pulse compression with glass: a new method of generating pulses shorter than 60 femtoseconds. *Optics Letters*, 8:4–6, 1983. 2

[4] J. J. Fontaine, W. Dietel, and J.-C. Diels. Chirp in a mode-locked ring dye laser. *IEEE J. of Quantum Electron.*, QE-19:1467, 1983. 2

[5] John L. Hall. Optical frequency measurement: 40 years of technology revolutions. *IEEE Journal on Selected Topics in Quantum Electronics*, 6:1136–1144, 2000. 2

[6] Th. Udem, R. Holzwarth, and T.W. Hänsch. Optical frequency metrology. *Nature*, 416:233–237, 2002. 3

[7] Scott A. Diddams. The evolving optical frequency comb [invited]. *J. Opt. Soc. Am. B*, 27:51–62, 2010. 3

[8] Ladan Arissian and Jean-Claude Diels. Investigation of carrier to envelope phase and repetition rate — fingerprints of mode-locked laser cavities. *Journal of Physics B: At. Mol. Opt. Phys*, 42:183001, 2009. 3, 4

[9] Ming Lai, Jean-Claude Diels, and Michael Dennis. Nonreciprocal measurements in fs ring lasers. *Optics Letters*, 17:1535–1537, 1992. 3

[10] M. L. Dennis, J.-C. Diels, and M. Mohebi. Study of a carbon dioxide ring laser gyroscope. *Applied Physics B*, B54:278–287, 1992. 3

[11] Matthew T. Hummon, Songbai Kang, Douglas G. Bopp, Qing Li, Daron A. Westly, Sangsik Kim, Connor Fredrick, Scott A. Diddams, Kartik Srinivasan, Vladimir Aksyuk, and John E. Kitching. Photonic chip for laser stabilization to an atomic vapor with 10−11 instability. *Optica*, 5(4):443–449, Apr 2018. 3

[12] Holly Leopardi, Josue Davila-Rodriguez, Franklyn Quinlan, Judith Olson, Jeff A. Sherman, Scott A. Diddams, and Tara M. Fortier. Single-branch er:fiber frequency comb for precision optical metrology with 10−18 fractional instability. *Optica*, 4(8):879–885, Aug 2017. 3

[13] Koji Masuda, James Hendrie, Jean-Claude Diels, and Ladan Arissian. Envelope, group and phase velocities in a nested frequency comb. *Journal of Physics B*, page in print, 2016. 11, 12, 13, 16, 17, 32

[14] J.-C. Diels and Wolfgang Rudolph. *Ultrashort laser pulse phenomena*. Elsevier, ISBN 0-12-215492-4; second edition, Boston, 2006. 18

[15] H. R. Telle, G. Steinmeyer, A. E. Dunlop, S. Stenger, D. A. Sutter, and U. Keller. Carrier-envelope offset phase control: A novel concept for absolute optical frequency measurement and ultrashort pulse generation. *Appl. Phys. B*, 69:327, 1999. 18

[16] Daniel A. Steck. Rubidium 87 d line data. available on line at http://steck.us/alkalidata (revision 2.1.1), 2009. 21, 22

[17] Xiao Xiang, Ziyue Zhang, Shaofeng Wang, Mengmeng Wang, Tao Liu, Ruifang Dong, Hainian Han, Shougang Zhang, and Zhiyi Wei. Carrier-envelope offset frequency stabilization of a 100 fs-scale ti:sapphire mode-locked laser for quantum

frequency comb generation. *Journal of Physics Communications*, 2(5):055031, May 2018. 30, 74, 76

[18] D. Fehrenbacher, P. Sulzer, A. Liehl, T. Kälberer, C. Riek, D. V. Seletskiy, and A. Leitenstorfer. Free-running performance and full control of a passively phase-stable er:fiber frequency comb. *Optica*, 2(10):917–923, Oct 2015. 31

[19] Teresa I. Ferreiro, Jinghua Sun, and Derryck T. Reid. Locking the carrier-envelope-offset frequency of an optical parametric oscillator without f–2f self-referencing. *Opt. Lett.*, 35(10):1668–1670, May 2010. 31

[20] K. Masuda, E.I. Vaughan, L. Arissian, J.P. Hendrie, J. Cole, J.-C. Diels, and A. Hecht. Novel techniques for high precision refractive index measurements, and application to assessing neutron damage and dose in crystals. *Nuclear Instruments and Methods in Physics Research Section A: Accelerators, Spectrometers, Detectors and Associated Equipment*, 784:198–201, 2015. 32, 33

[21] J. Hendrie, J.-C. Diels, and L. Arissian. Nested fabry-perot in mode-locked lasers to monitor minute changes of index. In *CLEO, 2015*, page SF2L.7, San Jose, CA, 2015. 33

[22] L. Arissian and J.-C. Diels. Intracavity phase interferometry: frequency comb sensors inside a laser cavity. *Laser Photonics Rev*, 8:799–826, 2014. 40

[23] Ladan Arissian and Jean-Claude Diels. Mode-locked laser applied to coherent interactions and phase measurements. *Journal of Modern Optics*, 53:2593–2603, 2006. 43

[24] Andreas Schmitt-Sody, Ladan Arissian, Andreas Velten, Jean-Claude Diels, and Dave Smith. Rabi cycling of two pulses in a mode-locked ring laser cavity with electro-optical control. *Physical Review A*, 78:063802, 2008. 43, 45

[25] J.-C. Diels, Jason Jones, and Ladan Arissian. Applications to sensors of extreme sensitivity. In Jun Ye and Stephen Cundiff, editors, *Femtosecond Optical Frequency Comb: Principle, Operation and Applications*, chapter 12, pages 333–354. Springer, New York, NY, 2005. 43

[26] J.-C. Diels and Ladan Arissian. Intracavity phase measurements and ultrasensitive sensors. In Des Raj Vij, editor, *Handbook of Optical Materials, Devices and Systems*, page In Press. American Scientific Publishers (USA), 2009. 43

[27] Scott Diddams, Briggs Atherton, and Jean-Claude Diels. Frequency locking and unlocking in a femtosecond ring laser with the application to intracavity phase measurements. *Applied Physics B*, 63:473–480, 1996. 43, 45

[28] J.-C. Diels and M. Lai. Bidirectional operation and gyroscopic properties of an homogeneously broadened ring laser. *Phys. Rev. A*, 44:5898–5903, 1991. 43

[29] Matthew J. Bohn and Jean-Claude Diels. Bidirectional Kerr-lens mode-locked femtosecond ring laser. *Opt. Comm.*, 141:53–58, 1997. 43, 45

[30] Matthew J. Bohn, Jean-Claude Diels, and R. K. Jain. Measuring intracavity phase changes using double pulses in a linear cavity. *Optics Lett.*, 22:642–644, 1997. 43, 44

[31] Ladan Arissian, Alex Braga, and Jean-Claude Diels. Differential beat note interferometry in linear lasers with two pulses/cavity round-trip. In *Photonics North 2008*, pages Optical fiber sensors OSD–3–4–2, Montreal, Canada, 2008. IEEE, UFFC. 43

[32] R. J. Jones and J. C. Diels. Stabilization of femtosecond lasers for optical frequency metrology and direct optical to radio frequency synthesis. *Phys. Rev. Lett.*, 86:3288–3291, 2001. 43

[33] Andreas Velten, Andreas Schmitt-Sody, and Jean-Claude Diels. Precise intracavity phase measurement in an optical parametric oscillator with two pulses per cavity round-trip. *Optics Letters*, 35:1181–1183, 2010. 43

[34] Xuan Luo. *Investigation of intracavity phase interferometry applied to femtometrology*. PhD thesis, The University of New Mexico, Albuquerque,New Mexico, 2014. 43

[35] Andreas Schmitt-Sody, Koji Masuda, Andreas Velten, and Jean-Claude Diels. Intracavity mode locked laser magnetometer. *Optics Communications*, 283(17):3339 – 3341, 2010. 43, 63

[36] J.-C. Diels. Detection of groundwater through ultra-sensitive magnetic measurements with ultra-short pulse lasers. WWRI Technical Report No. 313, February 2001. New Mexico Water Resources Research INstitute, NMSU, Box 30001, Las Cruces, NM 88003. 43, 63

[37] James Hendrie, Matthias Lenzner, Hanieh Akhamiardakani, Jean-Claude Diels, and Ladan Arissian. Impact of resonant dispersion on the sensitivity of intracavity phase interferometry and laser gyros. *Optics Express*, 24:30402–304010, 2016. 44, 50, 53, 54, 56

[38] J.-C. Diels and M. Dennis. Mode-locked active gyro solid state lasers. United States Patent, Filed June 28, 1991 1994. PATENT NUMBER 5,363,192. 44

[39] J.-C. Diels and M. Lai. Solid state laser gyro with interferometrically substracted noise. United States Patent, Filed July 28, 1991 1993. PATENT NUMBER 5,191,390. 44

[40] J.-C. Diels, Matt Bohn, Jason Jones, and Thien Trang Dang. Sensors of rotation, displacement, index of refraction, magnetic field, electric field and magnetic susceptibility. United States Patent, Filed April 27 2000. U.S. Patent Nb. 6,650,682. 44

[41] M. Lenzner J.-C. Diels, L. Arissian and J. Hendrie. Enhancement of the phase response of intracavity phase interferometers including laser gyro's. United States Patent 10317212, Approved June 11, 2019 2019. Patent Application Serial N0 15/984048. 44, 50

[42] M. G. Sagnac. L'éther lumineux démontré par l'effet du vent relatif d'éther dans un interféromètre en rotation uniforme. *Comptes Rendus*, 157:708–710, 1913. 47

[43] M. G. Sagnac. Sur la preuve de la réalité de l'éther lumineux démontré par l'expérience de l'interférographe tournant. *Comptes Rendus*, 157:1410–1413b, 1913. 47

[44] Chengyi Luo, Jiahao Huang, Xiangdong Zhang, and Chaohong Lee. Heisenberg-limited sagnac interferometer with multiparticle states. *Phys. Rev. A*, 95:023608, Feb 2017. 50

[45] Joseph M. Lukens, Nicholas A. Peters, and Raphael C. Pooser. Naturally stable sagnac–michelson nonlinear interferometer. *Opt. Lett.*, 41(23):5438–5441, Dec 2016. 50

[46] M. S. Shahriar, G. S. Pati, R. Tripathi, V. Gopal, M. Messall, and K. Salit. Ultrahigh enhancement in absolute and relative rotation sensing using fast and slow light. *Physical review A*, 75:053807, 2007. 55

[47] Tianliang Qu, Kaiyong Yang, Xiang Han, Suyong Wu, Yun Huang, and Hui Luo. Design of a superluminal ring laser gyroscope using multilayer optical coatings with huge group delay. *Nature Communications*, 2014. 55

[48] D. D. Smith, K Myneni, J. A. Odutola, and J.-C. Diels. Enhanced sensitivity of a passive optical cavity by an intracavity dispersive medium. *Physical Review A*, 80:011809(R), 2009. 55

[49] David D. Smith, H. A. Luckay, Hongrok Chang, and Krishna Myneni. Quantum-noise-limited sensitivity enhancement of a passive optical cavity by a fast-light medium. *Phys. Rev. A*, 94:023828, Aug 2016. 55

[50] Shin Arahira and Yoh Ogawa. Synchronous mode-locking in passively mode-locked semiconductor laser diodes using optical short pulses repeated at subharmonics of the cavity round-trip frequency. *IEEE Photonics Technology Letters*, 8:191–193, 1996. 69

[51] N. H. Bonadeo, W. H. Knox, Jeffrey M. Roth, and K. Bergman. Passive harmonic mode-locked soliton fiber laser stabilized by an optically pumped saturable bragg reflector. *Opt. Lett.*, 25(19):1421–1423, Oct 2000. 69

[52] M. Peccianti, A. Pasquazi, Y. Park, B.E. Little, S.T. Chu, D.J. Moss, and R. Morandotti. Demonstration of a stable ultrafast laser based on a nonlinear microcavity. *Nature Communications*, 3:765, 2012. 69

[53] D. W. Allan. Statistics of atomic frequency standards. *Proc. IEEE*, 54:221–230, 1966. 74

[54] J. E. Gray and D. W. Allan. A method for estimating the frequency stability of an individual oscillator. In *28th Annual Symposium on Frequency Control*, pages 243–246, May 1974. 74, 76

[55] C. A. Greenhall. Frequency stability review. *The Telecommunications and Data Acquisition Report*, pages 200–212, Feb. 1987. 74

[56] D. A. Howe, D. W. Allan, and J. A. Barnes. Properties of oscillator signals and measurement methods. `https://tf.nist.gov/phase/Properties/main.htm`, May 2019. 75, 76